Vortex avalanches in type II superconductors: the sandpile perspective

E. Altshuler

Superconductivity Laboratory, IMRE-Physics Faculty, University of Havana
10400 Havana, Cuba

I am never content
until I have constructed a mechanical model
of the subject I am studying.
If I succeed in making one, I understand;
otherwise I do not.

Lord Kelvin

A good mechanical model has the unique power to connect our intuition with the most abstract physical phenomena. Although purely mechanical systems may look old fashioned in contemporary Physics, the so called *granular state* has focused much attention in the last decade. *Avalanche dynamics* is one of the most fascinating features of some granular systems, and is present in other physical contexts, like *vortices in the slowly-driven critical state of type II superconductors*. After an introduction to the phenomenology of type II superconductivity and to sandpile physics, *key* experiments on vortex avalanches performed in the last five years are reviewed. Some new experiments on avalanche dynamics in superconducting, magnetic and other systems are suggested, in the philosophy of exploring mechanical analogies as far as possible –earthquakes included. Finally, some theoretical findings reported in the last three years on vortex dynamics achieved with the help of a simple cellular automaton (CA) model are reviewed, and further extensions of the model are proposed. This CA contains the essential ingredients that unify, at least to some extent, avalanche dynamics displayed by the superconducting and mechanical systems discussed in the paper.

PACS numbers: 45.70,45.70h,74.60w

Maxwell's "molecular vortices" in aether [1] constitute, perhaps, the most fruitful mechanical analog of electromagnetic phenomena ever conceived. It not only allowed him to understand the production of a magnetic field by an electric current and vice-versa as early as 1892, but led him to formulate the hypothesis of the existence of a displacement current and the epoch-making idea

of electromagnetic waves.

Even when Electromagnetism seemed complete at the turn of the century with the experimental work of Faraday and Maxwell's equations, electromagnetic fields in the Solid State would prove to be a fertile ground for devising ingenious mechanical analogies. The opening of the new era of Superconductivity in 1911, when Heike Kammerling Onnes reported the disapearance of electrical resistance below 4.2 K in mercury [2], is one example. While mechanical models have helped the understanding of superconductive phenomena, mechanical (or fluid-mechanical) systems displaying a close resemblance with superconductivity have seen their physics clarified with the help of superconducting theories, or are just developing in parallel. This is the case of superfluids and, particularly, of sandpiles, which are entering the XXI Century with a whole agenda of unanswered questions.

1. A Superconductivity primer

The first mechanical analog of Superconductivity is Superfluidity, a phenomenon that has only been observed for liquid helium [3]. The basic characteristic of both is their ability to sustain particle currents (being either superelectrons or superfluid particles) at a constant velocity for extended periods of time without any driving force. These currents are the only known examples of the motion of macroscopic systems without being quickly destroyed by dissipative processes. To describe the condensed particles in either system, we use a complex macroscopic wavefunction of the form:

$$\Psi(\vec{r},t) = \sqrt{n^*(\vec{r},t)}e^{i\theta(\vec{r},t)} \tag{1}$$

where n^* is either the number density of super-electrons or the density of the superfluid, and θ is the phase. It is straightforward from 1 that the amplitude squared of the wavefunction equals n_s. Although the analogy can be pushed further, we will present the next results only for the case of superconductors. Let us postulate that our macroscopic wavefunction obeys the Schrödingerlike equation

$$i\hbar\frac{\partial\Psi(\vec{r},t)}{\partial t} = \frac{1}{2m^*}\left(\frac{\hbar}{i}\nabla - q^*\vec{A}(\vec{r},t)\right)^2\Psi(\vec{r},t) + q^*\phi(\vec{r},t)\Psi(\vec{r},t) \tag{2}$$

where m^* and q^* are the superlectrons' mass and charge, respectively*, $\vec{A}$ is the vector potential, and ϕ is the scalar potential.

Simple manipulations involving equations 1 and 2, under the assumption of position and time independent n^*, give the so-called London equations [5]:

$$\frac{\partial}{\partial t}\left(\Lambda\vec{J}_s(\vec{r},t)\right) \approx \vec{E}(\vec{r},t) \tag{3}$$

*The standard microscopic theory of Superconductivity developed in 1957 by Bardeen, Schrieffer and Cooper [4] postulates that the superelectrons arrange themselves in pairs, so m^* and q^* are twice the mass and the charge of "normal" electrons, respectively. This picture seems to hold not only for the low temperature, but also for the new high temperature superconductors

$$\nabla \times \left(\Lambda \vec{J}_s(\vec{r},t)\right) = -\vec{B}(\vec{r},t) \tag{4}$$

where $\Lambda = \frac{m^*}{N^* q^{*2}}$, $\vec{E}$ and $\vec{B}$ are the electric field and magnetic field induction in the superconductor, and $\vec{J}_s$ is the superelectron current density. The first of these equations indicate that, if a constant current density is established along the superconductor, no voltage drop appears, as expected for a normal metal. In fact, this was the phenomenon observed by Kammerlingh-Onnes in 1911 for mercury when cooled below what he called the *critical temperature*, T_c. The second equation accounts for the so called Meissner-Oschenfeld effect [6]. These authors observed that, when a superconducting bulk sample was submitted to a constant magnetic field, and its temperature lowered below T_c, the average magnetic induction into the sample practically switched to zero. When solving equation 4 one can see that, in fact, the magnetic induction decays exponentially from the applied induction at the sample boundaries to virtually zero at its interior within a characteristic length, λ, known as the *London penetration depth*. This is due to the appearance of a shielding current which also decays exponentially from the surface within λ.

The combination of 1 and 2 also gives a third equation known as *fluxoid quantization law*, which reveals the quantum nature of the macroscopic wavefunction:

$$\oint_C \vec{J}_s(\vec{r},t)\cdot d\vec{l} + \int_S \vec{B}(\vec{r},t)\cdot d\vec{s} = n\Phi_0, \qquad n = 0,1,2... \tag{5}$$

where C is a closed path into the superconductor limiting a surface S which includes a non-superconducting inclusion piercing the superconductor in the direction of the applied magnetic field. The left hand of 5 is called *fluxoid*, and the equation says that it can only take integer values of the *flux quantum*, $\Phi_0 = 2,07 \cdot 10^{-15} Tm^2$. If C is wide enough, we can neglect the first term of the fluxoid, and then we can safely talk about *flux* quatization. The phenomenon was first observed by Doll and Näbauer [7] and by Deaver and Fairbank [8] in 1961. Equations 3, 4 and 5 are good enough to describe phenomenologically a *type I* superconductor.

Another consequence of postulates 1 and 2 when applied to a junction consisting in a thin insulating layer sandwiched between two superconducting electrodes is the so-called *Josephson effects* [9,10].A real junction can be modeled as an "ideal" junction in parallel with a capacitor (associated to the effect of the finite-area superconducting electrodes) and a resistor (associated to the "normal" electrons flowing through the junction due to thermal excitation and/or to excess applied current).The solution of this equation can be beautifully visualized by means of a mechanical analogue suggested by Anderson in 1964 [11] and worked out by Sullivan and Zimmerman in 1974 [12].

2. Vortices and the Critical State

2.1. *Vortices in ideal superconductors*

A more general approach to Superconductivity is the Ginzburg-Landau (G-L) theory [13]. It can be regarded as the application of Landau's theory of second-order phase transitions to the

case of superconductors, resulting in the so-called Ginzburg-Landau equations. In fact, *equation 2 is just a linearized form of one of them*. G-L theory can be conveniently modified to account for the case of superfluid He, giving the so-called Ginzburg-Pitaevsky equations [14]. It is perhaps the prediction of the existence of type II superconductors the most important result of G-L theory. Let us define the parameter

$$\kappa = \frac{\lambda}{\xi} \tag{6}$$

where ξ is the so-called *coherence length* (a lengthscale characterizing the maximum spatial variation of the superconducting wavefunction). Then, type I and type II superconductors correspond to the conditions $\kappa \leq 1/\sqrt{2}$ and $\kappa \geq 1/\sqrt{2}$, respectively. But the striking differences between type I and type II superconductors are best represented in their $H - T$ diagrams.

Figure 1a (left)displays the two phases corresponding to type I superconductors, separated by a line known as the *thermodynamic critical field*, $H_c(T)$. Under that line we find the "Meissner" phase ($\vec{B} = 0$ into the superconductor), while above there is the "Normal" phase, where the material is completely penetrated by the applied field.

Figure 1a (right) displays the diagram for a "low T_c" type II superconductor, in which three phases are observed, separated by two lines, $H_{c1}(T)$ and $H_{c2}(T)$, known as the *lower* and *upper* critical fields, respectively. While below $H_{c1}(T)$ and above $H_{c2}(T)$ type II superconductors behave qualitatively identical to type I, a new phase known as *mixed state* appears between them. In this region, the sample is *partially* penetrated by the applied field. Based on the G-L theory, Abrikosov proved, in 1957 that this penetration occurs as an hexagonal lattice of *vortices*, which are "mesoscopic" objects whose structure and basic properties will be discussed below [15]. Their existence was directly proved by Essman and Träubein in 1967 through Bitter decoration experiments [16].

Figure 2a shows a rough diagram of a vortex. It consists of a normal cylinder (or *core*) of radius ξ paralell to the direction of the applied field which is surrounded by "vorticial" superconducting currents decaying within a radius λ in such a way that they can be regarded as tiny concentric coils producing a magnetic induction in the same direction of the applied field (An alternative picture is that the vorticial currents prevent the Meissner phase outside the vortex to be "invaded" by the field inside it!).

Apart from G-L theory, a simple argument allows to calculate the flux associated to a single vortex. Considering the experimental fact that vortices in the mixed state arrange in an hexagonal lattice, it is easy to see that the mean magnetic induction of the system is

$$\langle B \rangle = \frac{2}{\sqrt{3}\alpha^2}\Phi_v \tag{7}$$

where α is the intervortex distance and Φ_v is the magnetic flux associated to each vortex. If we now apply the flux quatization condition 5 along a suitable path around the vortex, we get $\Phi_v = \Phi_o$. Then, *the magnetic flux associated to one vortex is a single flux quantum*.

Knowing the vortex structure, it is easy to get an intuitive picture of the mixed state close to its boundaries. Near $H_{c1}(T)$, the lattice constant is very large. As one approaches $H_{c2}(T)$,

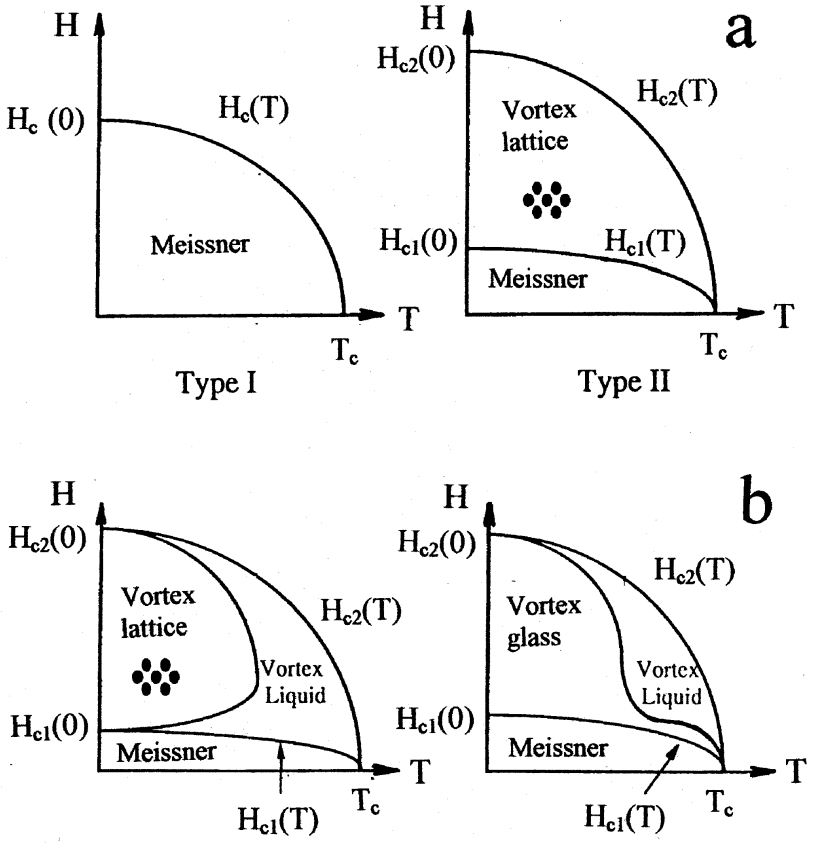

Figure 1: Magnetic phase diagrams for (a) low-T_c and (b) high-T_c superconductors. In (a), type I and type II superconductors correspond to the left and right graphs, respectively. In (b), two possible phase diagrams are represented for high-T_c materials.

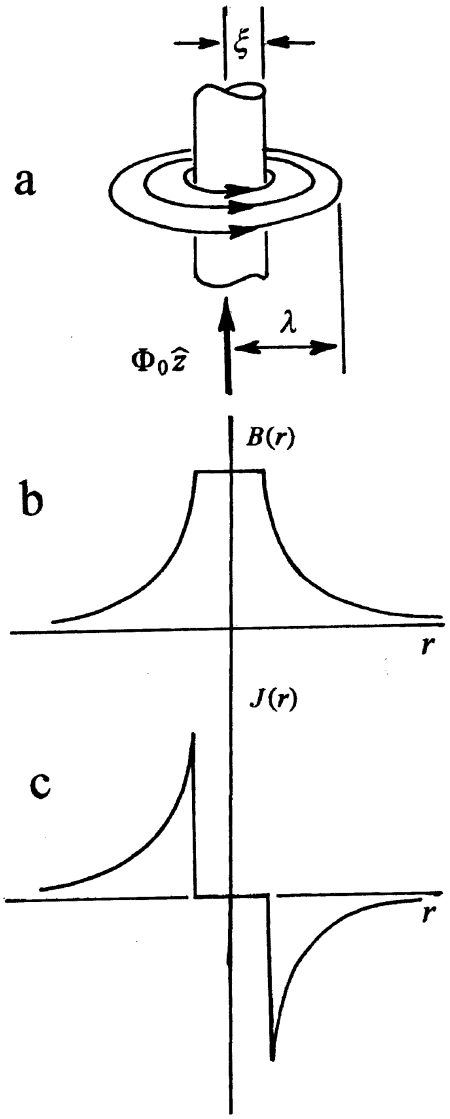

Figure 2: The isolated vortex. (a) Spatial representation of the vortex core and the vorticial supercurrents. (b) Simplified graph of the magnetic induction associated to the vortex. (c) Simplified graph of the supercurrents associated to the vortex.

vortices become increasingly crowded, and, very close to $H_{c2}(T)$, $\alpha \to \xi$: the whole system is nearly in the normal state.

Insisting in our phenomenological approach, we can get reasonable approximations for $B(r)$ and $J_s(r)$ for a single vortex by conveniently modifying London equation 3. The results are qualitatively illustrated in Figure 2b,c assuming cylindrical coordinates. We can also get the following expression for the *electromagnetic energy per unit length of the vortex* [17]:

$$E_v = \frac{\Phi_0^2}{4\pi\mu_0\lambda} K_0(\frac{\lambda}{\xi}) \tag{8}$$

where $K_0(\frac{\lambda}{\xi})$ is the zeroth-order modified Bessel function, that can be approximated by $ln(\frac{\lambda}{\xi})$ if $\lambda \gg \xi$. We can also estimate the interaction energy per unit length between two paralell vortices with fields pointing in the same direction (we will call them just *paralell* vortices)[17]:

$$E_{vv} = 2E_v - \frac{\Phi_0^2}{4\pi\mu_0\lambda^2} K_0(\frac{l}{\xi}) \tag{9}$$

where l is the intervortex distance . It can be easily seen that the first term of the right corresponds to the simple superposition of the individual vortex energies per unit length, so the last term is the interaction energy. Its minus sign indicates that *two paralell vortices repel each other*. If we calculate the force of interaction per unit vortex length through the gradient of E_{vv} in the direction of the interaction, we get:

$$f_{vv} = -\frac{\Phi_0^2}{2\pi\mu_0\lambda^3} K_1(\frac{l}{\xi}) \tag{10}$$

where $K_1(\frac{l}{\lambda})$ is the modified Bessel function of the first order. Again, the minus sign indicates repulsive interaction.

This interaction can be also visualized coming back to our superfluid analogy. The upper part of Figure 3a shows the current lines of two superconducting vortices, and the lower part displays the flow pattern resulting from their superposition (the crosses indicate that the field enters the paper). Following elementary hydrodynamic arguments, a high pressure region appears between the vortices (due to the low transversal fluid velocity in that region), while low pressure regions appear at both sides (related to the high transversal fluid velocity there). This pressure map makes the vortices to repel each other. In fact, *superfluid vortices do exist in helium* [18].

Besides the three-dimensional "straight" ones discussed above, a rich zoology of vortices have been studied. One of these are the "doughnut-shaped" or "circular" vortices firstly discussed by Tinkham [19] and quite intensively re-visited in the nineties [20,21,22,23,24,25]. In contrast with straight ones, *circular vortices are unstable at zero applied field* because of their tendency to "shrink out" looking for energy minimization. As in the case of straight vortices, this effect can be also visualized dynamically: the vorticial doughnut can be sectioned into straight vortices of infinitesimal length. Then, each infinitesimal vortex attracts its "anti-paralell" mate at the other extreme of the corresponding diameter, provoking the shrinking of the doughnut. Other peculiar types of vortices appear in anisotropic superconductors, where λ and ξ are different along two

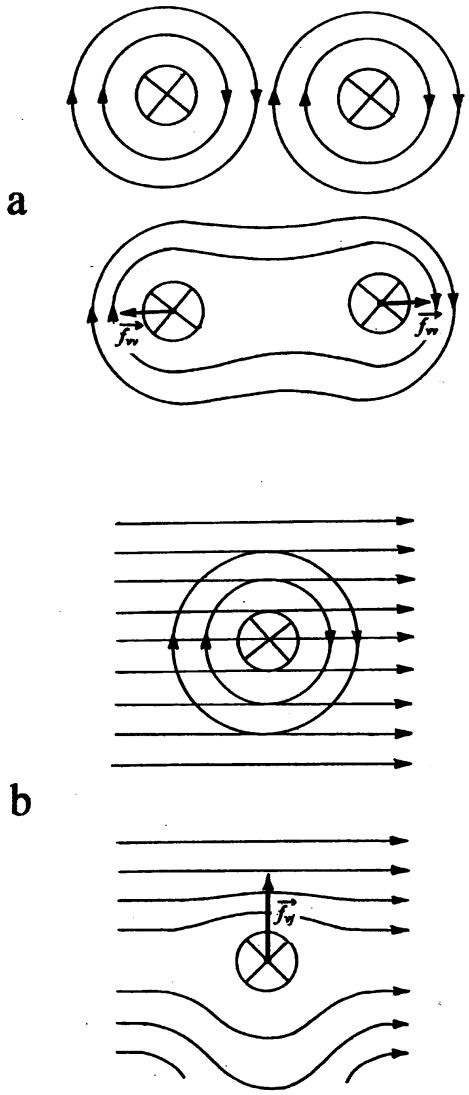

Figure 3: (a) Current superposition which illustrates the origin of the repulsive interaction between two vortices. (b) Current superposition which illustrates the origin of the force exerted on a vortex by a transport current.

perpendicular directions of the crystal. This can produce vortices with ellipsoidal instead of circular crossection, for example. The "High Temperature Superconductors"(or "HTc's") discovered by Bednorz and Müller in 1986 [26] and rapidly enriched and developed by others [27,28,29,30] are "extreme" anisotropic superconductors. In fact, they can be modelled as arrays of paralell superconducting layers along the ab planes of the structure (called "CuO planes") alternating with non-superconducting layers. When a current flows perpendicular to these layers, the system can be treated as a stack of Josephson junctions. If a magnetic field is applied perpendicular to the CuO-planes ($H \perp ab$), *two-dimensional* "pancake" vortices appear laying in the CuO planes which eventually form stacks in the direction of the field (Figure 4a) [31,32,33,34]. If the field is applied paralell to the ab planes ($H \parallel ab$), vortices appear involving both supercurrents along the ab planes, and Josephson currents perpendicular to the ab planes (Figure 4b) [35,36,37,38,39,40,41].

Let us return to simple three-dimensional straight vortices and examine their interaction with a transport current of density $\vec{J}$. Considering that a vortex carries a flux quantum, it can be shown that it experiences a "Lorentz-like" force per unit length of the form:

$$\vec{f_{vj}} = \vec{J} \times \Phi_0 \vec{i_z} \tag{11}$$

where $\vec{i_z}$ is the unit vector in the direction of the vortex magnetic field. Again, our hydrodynamic analog allows us to visualize the situation. The upper part of Figure 3b displays the straight current flow lines and the vorticial lines, while the lower part shows their superposition. Then, high and low pressure regions develop on the bottom and top sides of the vortex, respectively, causing a force pointing upwards. This, of course, follows the vector product of equation 11 if the flow is identified with $\vec{J}$ and the vortex comes out of the paper. The movement of a vortex caused by this force is known as *flux flow*. As demonstrated by Bardeen and Stephen [42], *flux flow is a dissipative process* because of the existence of a viscous drag per unit length opposed to $\vec{f_L}$, related to the scattering of superelectrons at the core boundary when it moves. Phenomenologically, the magnitude of the drag force can be roughly expressed as

$$f_D = \eta v_v \tag{12}$$

where η is a drag coefficient which depends on the core details, and v_v is the vortex velocity.

Let us integrate now all vortex interactions for the case of a sample in the mixed state submitted to an external magnetic field. First, the Abrikosov lattice can be thought as the *equilibrium* result of the vortex-vortex interactions into the sample –which try to push them off the sample– plus the interaction between these vortices and the external field (thought as a "vortex continuum" outside the sample) –which tries to push the vortices inside–. If we now introduce a transport current pointing upwards, and we assume that the field comes out of the paper, each vortex will suffer an extra force of identical magnitude and direction, so *the whole lattice will move to the right.*

All in all, each vortex in the lattice experiences a *net* force per unit length of magnitude:

$$f_T = J\Phi_0 - \eta v_v \tag{13}$$

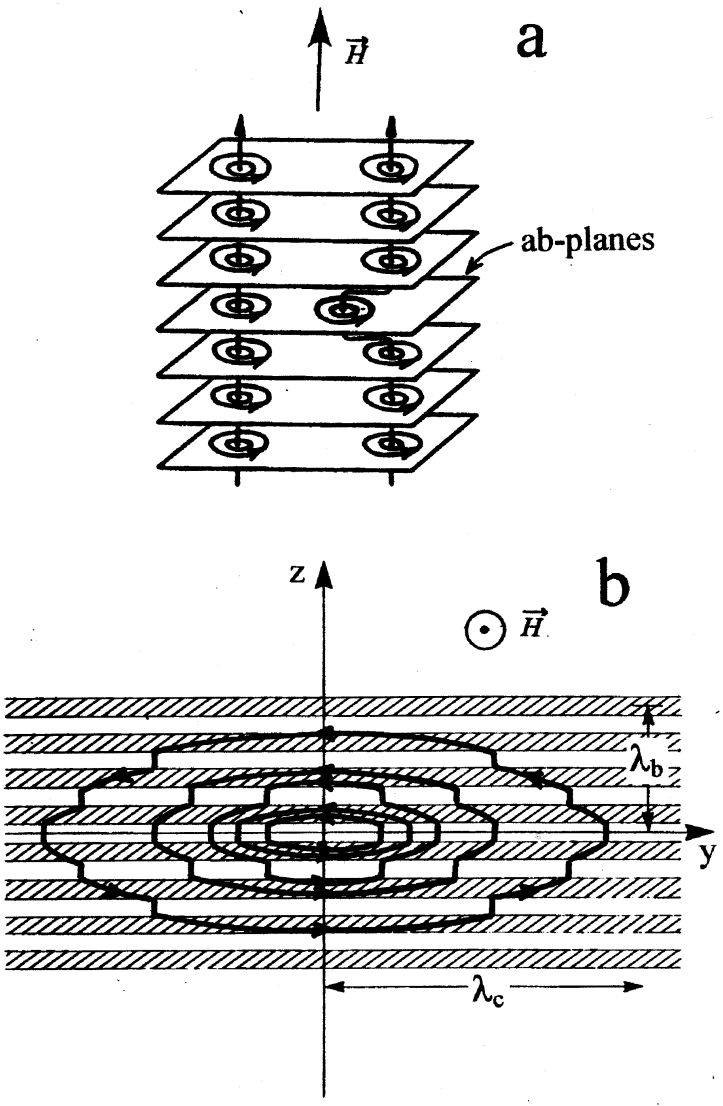

Figure 4: (a) Arrays of pancake vortices associated to a magnetic field applied perpendicularly to the "ab planes" of a high-T_c superconductor. (b) Josephson vortex associated to a magnetic field applied paralell to the "ab planes" of a high-T_c superconductor.

Note that the (equilibrium) vortex-vortex forces associated to its neighbors cancel out due to the symmetry of the Abrikosov lattice so they do not appear in 13. A naive conclusion from this is that the application of a transport current in the mixed state would immediately produce dissipation, so the critical current —defined as the maximum applied current that a type II superconductors in the mixed state can stand without dissipation— would be zero. This is not the case in the experiment, as we will see in the next section.

2.2. *Vortices in real superconductors*

2.2.1. *Pinning and $J-V$ curves*

Point defects, dislocations, second-phase inclusions and other defects make real superconductors inhomogeneous, in contrast to "ideal" superconductors. Let us model an inhomogeneity as a non-superconducting infinite cylinder of radius ξ and consider its interaction with a vortex paralell to the cylinder.

It is not difficult to see that it is energetically favorable for the vortex core to set just on the defect, since, in principle, the creation of the normal core in the Meissner sea has an energy cost which is "relieved" if the core finds an "already normal" location. If this is the situation, it is said that the vortex is *pinned* by the defect, which is then called *pinning center*. The energy needed for extracting a vortex from a pinning center is known as *pinning energy*. The approximate pinning energy per unit vortex length can be expressed, in the case of the defect described above, as:

$$U_P = \frac{1}{2}\mu_0 H_c^2 \pi \xi^2 \tag{14}$$

where H_c is the thermodinamical critical field. It should be noted that other inhomogeneities such as cylindrical defects with radius bigger or smaller than ξ, spherical defects, or planar ones, are "less efficient" pinning centers (i.e., have smaller pinning energies). The minimum force needed to extract a vortex from a pinning center is called *pinning force*. The pinning force per unit vortex length for our model defect can be readily estimated from 14 as:

$$f_P = \frac{U_P}{2\xi} \tag{15}$$

Of course, the real picture must include the whole Abrikosov lattice, for which we have to solve the problem of the *summation of pinning forces*, which is highly nontrivial in the presence of random pinning [43]. To get rid of this complication, let us assume the very unrealistic situation of one pinning center per vortex, and equal pinning strengths for all centers. Then, we can define the *critical current density* in the mixed state of a type II superconductor with pinning that which produces a Lorentz-like force strong enough to depin the lattice, i.e.:

$$f_P = J_c \Phi_0 \Longrightarrow J_c = \frac{f_P}{\Phi_0} = \frac{U_P}{2\xi\Phi_0} \tag{16}$$

This result solves the pretended contradiction at the end of the last section. It also indicates that, for type II superconductors with pinning, the total force can be expressed as:

$$f_T = J\Phi_0 - \eta v_v - J_c\Phi_0 \tag{17}$$

and the vortex velocity in the steady state (i.e., $f_T = 0$), as:

$$v_v = \frac{1}{\eta}(J - J_c)\Phi_0 \tag{18}$$

The application of Faraday's law indicates that the voltage dissipation due to vortex motion is proportional to its velocity, so it can be written as:

$$V = (J - J_c)\rho_{ff}h \tag{19}$$

where h is the distance between voltage probes in the direction of the transport current, and ρ_{ff} is called *flux flow resistivity*

In conclusion, if we apply an increasing transport current through the extremes of a real type II superconductor in the mixed state with the field applied perpendicular to the current, and we measure the voltage drop through a second pair of (inner) contacts, as shown in Figure 5a, we find a $J - V$ curve like that shown in figure 5b (dotted line).

2.2.2. *The critical state*

Let us examine how vortices distribute into a type II superconducting slab of infinite dimensions along y and z submitted to a magnetic field $-\mathbf{z}H$, as represented at the right of Figure 6. As the field exceeds H_{c1}, vortices enter through the surface.

Assuming that each vortex inside the slab is located at a pinning center, it suffers two opposite effects: a "magnetic pressure" pushing it into the superconductor, and a pinning force opposite to its . This is illustrated in the top view of the slab depicted at the upper part of Figure 6 (the slab has been represented as finite along x and also along y for didactical reasons). This competition provokes a nonuniform distribution of vortices, i.e., the vortex density is highest at the boundaries, and decreases when we get into the sample. A practical way to represent this situation is to substitute the effect of the individual vorticial currents by the effective "macroscopic" currents resulting from their superposition –as represented in Figure 6- that can be thought of responsible for the " Lorentzlike" force acting on the vortex cores.

Charles Bean proposed, back in 1964 [44] that the entire system would organize itself in such a way that those currents would match the critical current density of the superconductor so the magnetic induction at a given point $\vec{r}$ is given by Ampere's law:

$$\left|\nabla \times B(\vec{r})\right| = \mu_0 J_c \tag{20}$$

It is worth noting that $B(\vec{r})$ is a *mesoscopic* quantity in the sense that it is the average magnetic induction over many vortices around the position $\vec{r}$, but it is not the thermodynamic induction averaged over the whole sample. This model is often referred in the literature as the *critical state model*. In its original approach, Bean also assumed that J_c was independent from the local induction, i.e., from $\vec{r}$. Under these conditions, it is easy to see that the current and

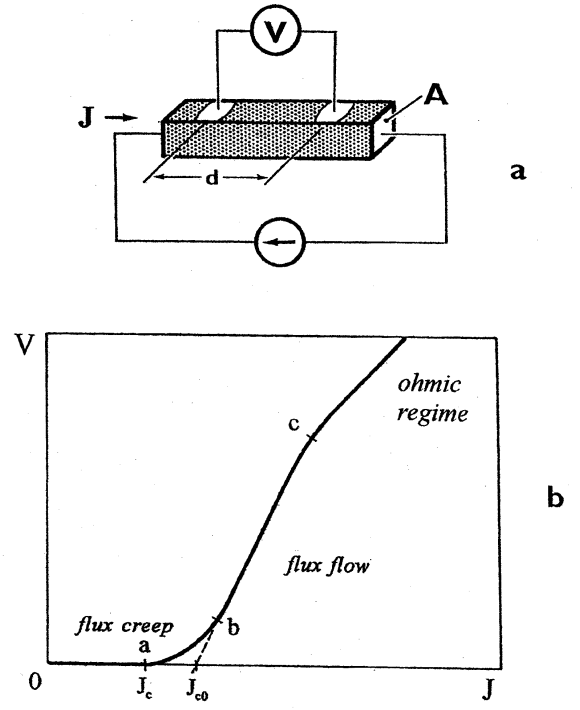

Figure 5: (a) Illustration of the "four probe arrangement". (b) Typical J-V curve measured with the arrangement depicted in (a) on a low-T_c superconductor.

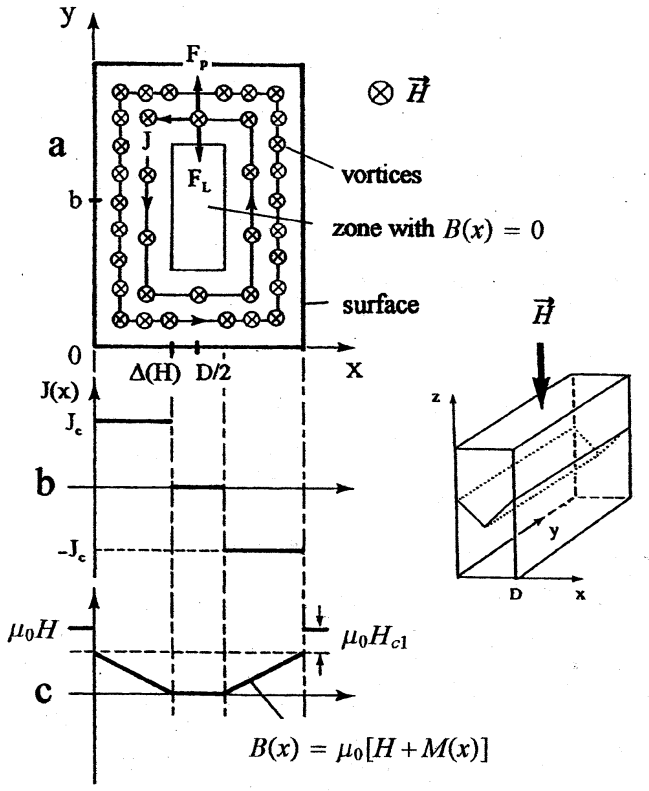

Figure 6: The critical state in type II superconductors. (a) Top view of a superconducting slab submitted to a magnetic field entering the page in which vortices are represented by crosses. (b) Current profile and (c) magnetic induction profile associated to the vortex arrangement depicted in (a). At the right, a simplified three dimensional representation of the magnetic induction profile into the sample. H_{c1} has not been neglected, as in the original model [44] .

magnetic field induction of our slab along x are the ones depicted in Figure 6 (note that the gap of the magnetic induction at the sample's surface is due to the presence of the London diamagnetic currents, which are not commonly taken into account in critical state models).

The module in equation 20 implicitly expresses a third hypothesis related to the "memory" of the material regarding how the magnetic field was applied. This hypothesis can be expressed like this: *the variations in the external field affect the vortex distribution from the sample boundaries to its interior, in such a way that different sections of the flux profile have slopes proportional either to J_c or to $-J_c$.* This nontrivial fact is better illustrated through a practical example as that depicted in the upper part of Figure 6, where the sample has been submitted to a field increase from zero to a certain H_m, and then to a field removal. Observe that the shielding capacity of the sample is not given by an increase of the magnitude of the shielding current –since $J = J_c$ everywhere–, but by the *volume* available for the flow of this current. Then, the maximum shielding capacity is reached in diagram 3 (see Figure 7), in which the external field has reached the value $H = H^* + H_{c1}$, where H^* is often called *full penetration field.* When the external field starts to diminish, the critical state at the "inner core" remains unchanged, while the vortices start to abandon the sample through the boundaries. This finally gives a profile like that depicted in diagram 8. However, it should be noted that the history can be very different if a lower H_m value is applied. The thermodynamic magnetization –i.e., that measured in typical magnetometric experiments– can be calculated, for our geometry, as:

$$M(H) = \frac{\langle B(x) \rangle}{\mu_0} - H = \frac{\int_0^D B(x)dx}{\mu_0 D} - H \tag{21}$$

for the particular magnetic history of Figure 7, the resulting $MvsH$ diagram is shown on its lower part.

It is worth noting that Bean's hypothesis $J_c \neq J_c(H)$ is not essential to critical state models. In fact, different $J_c(H)$ dependencies have derived in other models such as the "Kim model" [45] and the "exponential model" [46]. In our opinion, the critical state model is a major triumph of physical intuition with a certain " engineering" flavor, which was originally conceived without the knowledge of the existnce of vortices. Even when it has been extensively enriched for decades [47], the elucidation of the precise dynamics involved in its *establishment* –specially that related with vortex avalanches– as a scientific challenge both from the experimental [48,49,50,51,52,53,54,58,55,56,57] and from the theoretical [59,60,61,62,63,64,65,66,67,68,69,70,71,72] points of view. We will discuss in detail some of these works below.

Flux Creep

The previos decription of the critical state is basically correct at zero Kelvin. At finite temperatures, thermal activation can make the vortices –or vortex bundles– jump out of their pinning centers, redistributing into the sample in such a way that the Bean's profile changes in time, and, consequently, the shielding currents and sample magnetization. This phenomenon –known as *flux creep*– was firstly observed by Kim et al on the relaxation of persistent currents in NbZr tubes

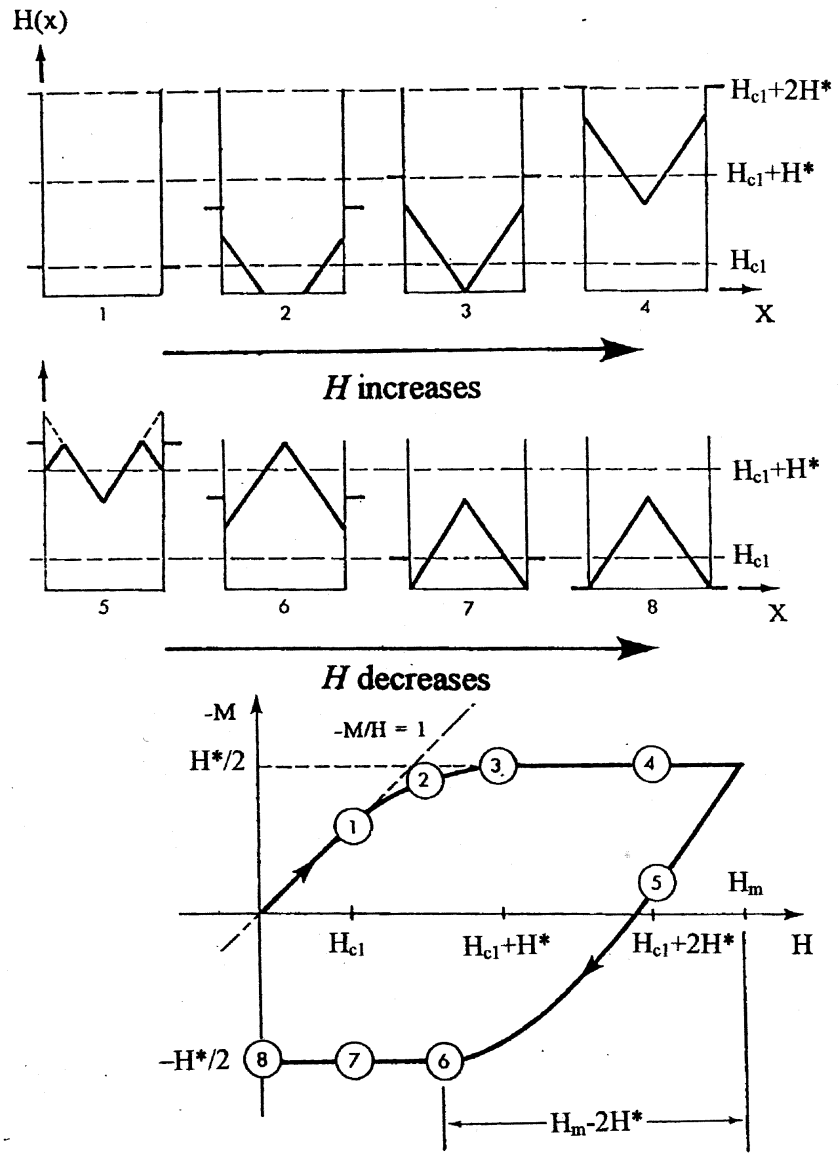

Figure 7: Magnetization derived from the critical state. Eight magnetic field critical state profiles corresponding to eigth values of the external field are illustrated at the upper part of the figure, and the corresponding points in the magnetization curve are depicted below. H_{c1} has not been neglected, as in the original model [44].

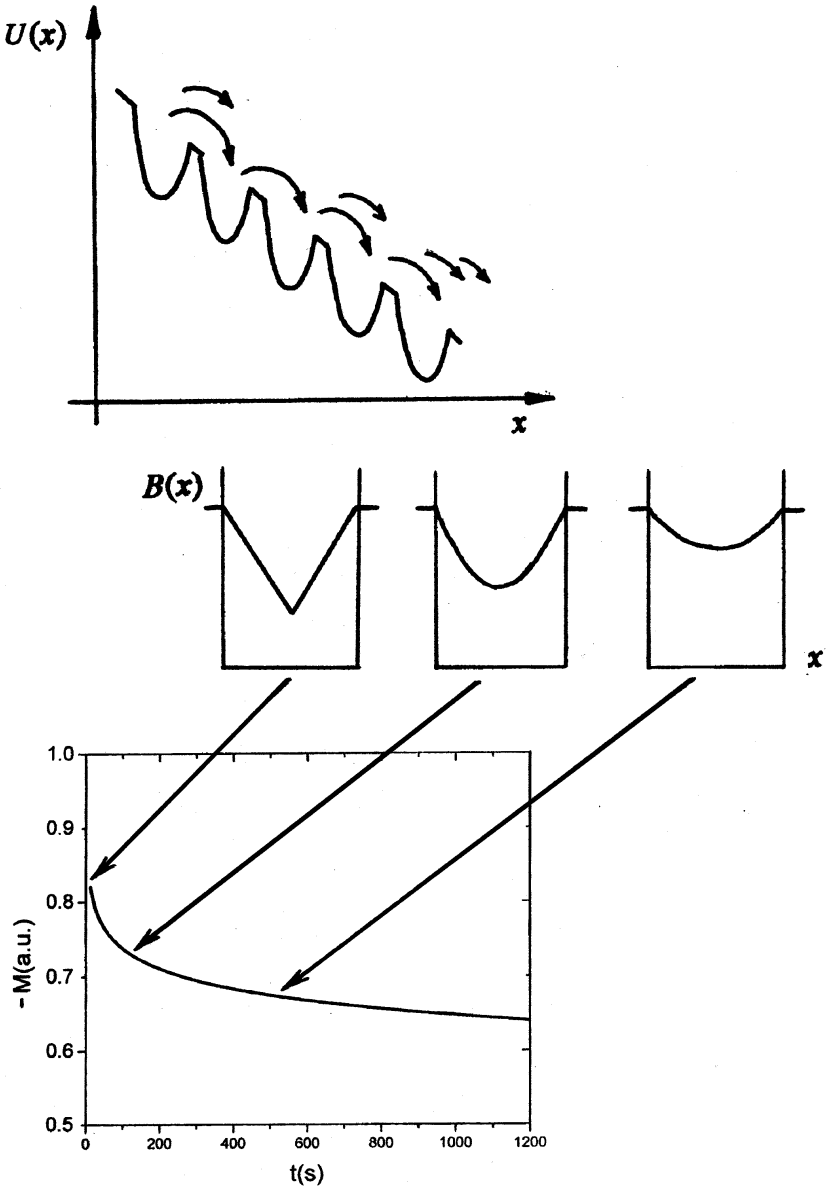

Figure 8: The upper part illustrates the "washboard" potential of pinning centers which provokes vortices to *creep* when thermally activated (vortex movement is represented by arrows). The resulting temporal evolution of the magnetic induction into the superconductor is qualitatively illustrated in the middle, which is connected to a *flux creep* measurement with illustrative purposes.

[74] and explained by Anderson and Kim [76] Their model –widely known as *Anderson-Kim model*– assumes that vortices jump off the pinning centers at an average frequency given by the Arrhenius relation $f = f_0 e^{-U/kT}$ were f_0 is an "effective attempt frequency", k is Boltzmann's constant, T is the temperature, and U is the pinning energy. Since the vortices are submitted to a Lorentz force in the critical state, it is clear that they basically jump out of the pinning centers in the direction of the Lorentz-like force. This situation can be represented by " tilting" the pinning wells in such a way that vortices "see" a lower potential barrier in the direction of the Lorentz-like force and a higher barrier in the opposite. The potential landscape that thermal activation encounters is often called "washboard potential", and is represented in the upper part of Figure 8. In the original Anderson-Kim approach [76] the pinning energy takes the form $U(J) = U_0(1 - J/J_{c0})$ where U_0 is the pinning potential in the absence of Lorentz-like forces (i.e., no flux gradient) and J_{c0} is the critical current density at $T = 0K$. In the case of low thermal activation ($U_0 >> kT$), these hypotheses give the following approximate formula for the relaxation of the shielding currents in the critical state:

$$J = J_{c0}[1 - \frac{kT}{U} ln(\frac{t}{t_0})] \tag{22}$$

where $t_0 \sim 1/f_0$. Taking into account equations 20 and 21, a similar decay can be derived, in a first approximation, for the macroscopic magnetization:

$$M = M_0[1 - \frac{kT}{U} ln(\frac{t}{t_0})] \tag{23}$$

where M_0 is the initial magnetization. This formula is only valid for "Fully penetrated samples", i.e., flux profiles like those depicted in diagrams 3 or 4, Figure 7.

The temporal relaxation of the magnetization is observed experimentally both in low and in high T_c superconductors. Figure 8 shows, in its middle section, how Bean's profiles "relaxes" in time due to thermally activated vortex jumps from the high to the low flux density regions in the sample. In Figure 8, a correspondence has been established between this process a fit to a relaxation experiment on a YBCO crystal performed with a Vibrating Sample Magnetometer [77] with didactical purposes. Although the Anderson-Kim approximation given by formula 23 is quite accurate for $U >> kT$ –which is a common situation in low-T_c supercondcutors–, typical results for High T_c are better described by nonlinear dependencies of the pinning potential such as $U(J) \propto [1 - (J/J_{c0})]^{3/2}$ [78], $U(J) \propto U_0[(J/J_{c0})^{\mu} - 1]$ [79] and $U(J) \propto U_0 ln(J_{c0}/J)$ [80] (observe that the last two pinning energies diverge as J approaches 0, which can be understood on the basis of *collective pinning theory*. In fact, High Temperature superconductors gave new life to flux creep phenomena, due to the very high creep rates they exhibit, called "giant flux creep" after Yeshurum and Malozemoff [81]. For an excellent review of the subject, the reader can consult [82].

Finally, it is worth noting that flux creep effects are also present in transport measurements. For example, in the case of an homogeneous type II superconductors, they are responsible for the exponential "rounding" of the J-V curves before J_{c0}, as depicted in Figure 5. More complex phenomena can take place in the case of inhomogeneous superconductors [83].

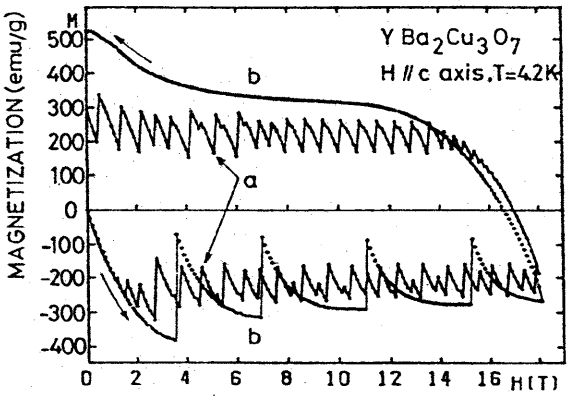

Figure 9: Magnetization loop showing *flux jumps* taken from [90]. (a) Sample in liquid He bath. (b) Sample in exchange gas.

Flux Jumps

As said before, the *attainment* of the critical state when ramping up (or down) the applied magnetic field is far from being well understood. One of the related phenomena that has attracted most interest due to its great technological relevance for the design of superconducting magnets, is the appearance of the so called *flux jumps*. They have been observed both in low T_c [84,85,86,87] and in High T_c superconductors [88,88,89,90,91,92,93,94,95,96,97]. The current interest in the phenomenon is illustrated by a very recent study of flux jumps in Nb films which reveals their correlation with the shape of the magnetization curve [57].

Flux jumps can be defined as thermodynamic catastrophes leading to the full or partial loss of magnetization in the superconductor. These events are the result of a positive feedback loop: as the external field is increased, vortices move to "reacommodate" in the sample, provoking heat dissipation through a Bardeen-Stephen mechanism [42]. If the magnetic diffusivity of the material is higher than the thermal one, this situation produces a temperature rise which, in turn, diminishes the critical current density, allowing the entrance of extra magnetic flux, which closes the feedback loop. It is intuitively clear that this process depends on the "intrinsic" thermal properties of the sample (specific heat and thermal conductivity), as well as on some "extrinsic" ones (sample size and quality of the thermal link with the sample holder). It also depends on how the critical current density depends on temperature and applied field, and how fast the external field is ramped.

The following conditions can give rise to the appearance of flux jumps: *"big" samples with poor thermal links with the sample-holder, magnetic fields applied at high ramp rates, strong temperature dependence of the critical current density, poor thermal conductivity, and low specific*

heat. Taking into account that the specific heat increases with temperature for high temperature superconductors (see, for example, reference [97]), *one concludes that very low temperatures are a nice scenario for flux jumps in* $HT_c's$.

As an example, Figure 9 shows magnetization loops with flux jumps measured by Guillot and coworkers [90] on a "large" YBCO crystal at 4.2 K with the magnetic field applied along the c-axis at a ramp rate of $300\,Oe/s$. Flux jumps are more dramatic for curve (b) (sample cooled with exchange gas) than for curve (a)(sample immersed in liquid helium), illustrating the effect of the thermal linkage of the sample. Some of these properties are contained in a *stability parameter*, β, usually defined to characterize thermally-triggered flux jumps [98].

It is important to note that, despite that no systematic special effort has been historically devoted to the study of their size and temporal statistics, flux jumps are regarded by most authors as a "rather periodic" event [88]. Some researchers have even defined a "frequency of magnetothermal oscillations" to describe flux jumps for a HT_c granular sample [97].

3. Sandpiles: new physics for old phenomena

In general, granular matter behaves differently from solids, liquids or gases. So it is not strange that some of the brightest minds in Physics of the XVIII and XIX centuries such as Coulomb [99], Faraday [100] and Reynolds [101] devoted some efforts to the understanding of granular systems. The strange fact is that the last decade of the XX century has concentrated most of the historical efforts to approach granular matter from a physical perspective, which has been described in several reviews [102,103,104,105,106,107,108,109,110,111,112,113,114,115]. This is connected, to some extent, with the use of sandpiles as the paradigm of *Self Organized Criticality* (SOC), a theory proposed by Bak and coworkers in 1987 [116] to explain a wide spectrum of natural phenomena, specially the so called "$1/f$" noise in many physical systems... even when the applicability of the paradigm cannot be fully demonstrated on *real* sandpiles.

Sandpiles constitute a beautiful mechanical analog of the critical state of type II superconductors, an idea first sketched by DeGennes in his 1966' classic book "Superconductivity of Metals and Alloys" [59]. As sand is added on a flat horizontal surface, the gravitational force tends to bring the grains down, while the frictional forces between grains prevent its action. The result of this competition is the building of a *pile*, characterized by an *angle of repose* or *critical slope*, which basically depends on the effective intergrain friction, and the friction between the grains and the flat surface. Of course it also depends on gravity, but it is usually a constant in "conventional" experiments (however, the rotation of the piles around a vertical axis, their immersion in some fluid, the tilting of the flat surface on which the pile is built, or an –expensive!– experiment in the Moon are examples of how to control also the "gravitational" forces). This situation remainds us of the description of the critical state of superconductors of section 2.2.2: the grains can be regarded as the vortices, the role of pinning is played by the intergrain friction, and the Lorentzlike force is analogous to the gravitational one.

Even when "everyday" conical sandpiles of "inverted V" shape are good enough for describing

the analogies with the critical vortex state, more elaborated piles must be built to resemble typical increasing-field Bean's profiles. This was didactically exploited by Campbell and Evetts in 1972 [43] to illustrate the influence of the sample *shape* in the resulting critical state profiles. The top picture of Figure 10 shows our own version of the sandpile critical profile equivalent to Diagram 4, Figure 7. It was obtained by evenly adding sand, through its two longer edges, to a rectangular box with open top and bottom faces which represents the superconducting sample: the sand profile inside the box mimics the critical state into the superconductor. The middle picture in Figure 10 represents the situation when the box is lowered relative to the sand it contains, allowing some of it to exit through the edges. The sand landscape into the box now resembles diagram 5 of Figure 7. Observe how the finiteness of our box produces critical slopes in two perpendicular directions.

To finish the presentation of the "static" analogies between sandpiles and the critical state of superconductors, it should be noted that two-dimensional (2D) sandpiles (we are using this term to describe conical piles or the ones formed into our sandbox) generally have quite linear profiles, which nicely adapt to the original *Bean* critical state model [44]. In the case of one-dimensional (1D) piles (we are using this term to describe piles formed between two vertical plates separated by the size of one grain), "kink" profiles and "logarithmic tails" are observed [117], as well as other complex structures [118]. To the author's knowledge, no 1D-critical state has been studied in the case of vortices to check if the analogy still works.

Not only static, but also some *dynamic* properties can be compared between sandpiles and critical vortex states. One of them is *relaxation*. Jaeger and Nagel, for example, measured in 1989 the temporal evolution of the angle of repose of a *slowly driven* sandpile †submitted to vibrations produced by an audio speaker [119], trying to mimic the effect of thermal activation on the critical state of a superconductor. The angle of repose decayed *logarithmically* in time within a range of vibration intensities, as the magnetization does in typical flux creep experiments (see section 2.2.2). The authors used an analogy of Anderson-Kim's flux creep model [76] to explain their results. It is still an open question, though, which property of the loudspeaker vibration (i.e., amplitude, frequency, mechanical power injected into the system, etc.) should be identified with thermal activation in vortex creep experiments. Moreover, the analogue of *temperature* is not very clear in the case of a sandpile [120] from a formal thermodynamic perspective. In any case, this example illustrates how the superconducting knowledge can shed some light on granular phenomena, as we suggested in the second paragraph of this paper. The bottom picture of Figure 10 illustrates the effect of gentle vibrations on the "decreasing field" sand profile shown in the middle picture. Observe the decreasing of the slopes, and the "rounding" of the edges, reminescent of the intermediate diagram of Figure 8 dealing with flux creep in type II superconductors (the "emergence" of a few big impurities which were originally buried in the sand illustrates one of the most characteristic phenomena of granular media: the so-called "Brazil nut seggregation" [121]).

But perhaps the most motivating dynamical analogy between sandpiles and the superconducting critical state was also drafted by DeGennes back in 1966 [59]: *the critical slope of a sandpile to*

†The term is used in the sense that a new grain is added to the pile only after the relaxation provoked by the previous addition has concluded.

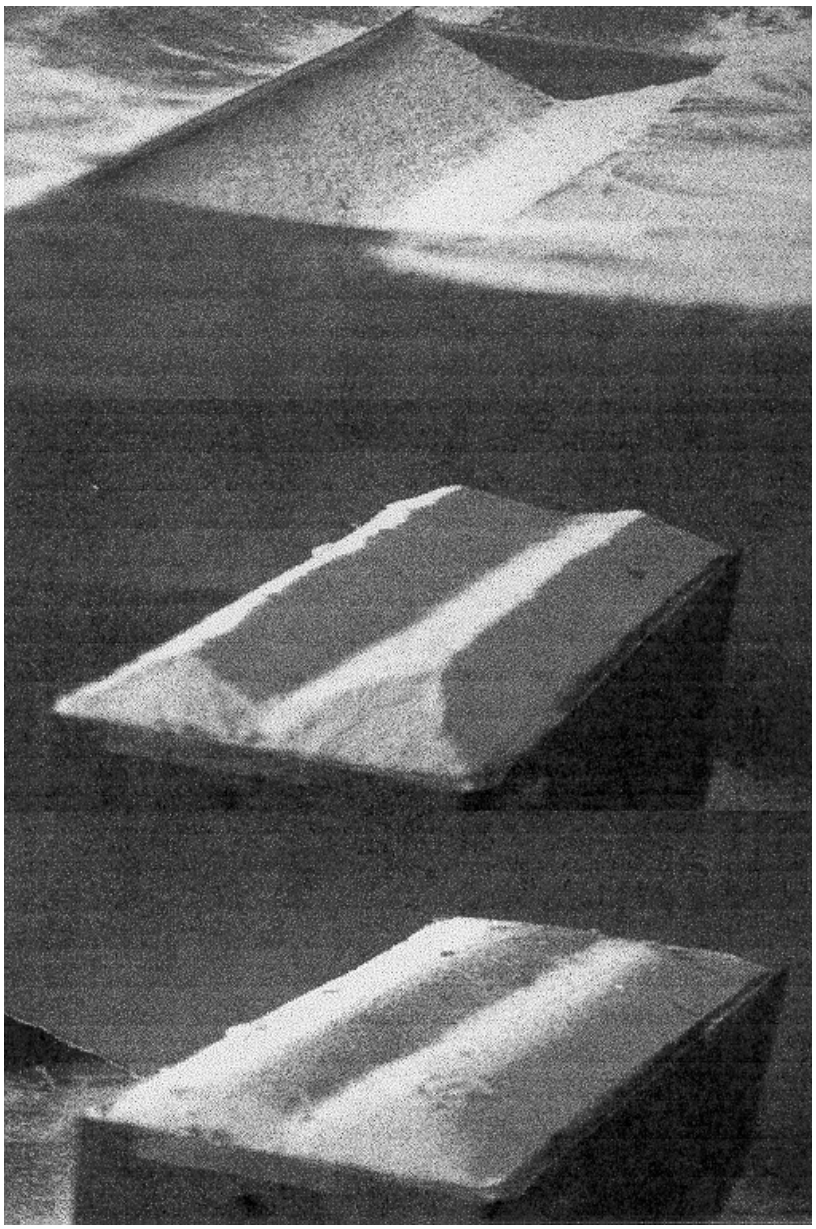

Figure 10: Sandpile analogues of two different stages of Bean's critical state model. Top picture: increasing field. Note similarity with the diagram at the right of Figure 6. Middle picture: decreasing field. Bottom picture: middle profile after "thermal" activation.

which grains are added is manitained through sand avalanches, and it seems reasonable to expect a similar dynamical behavior for the case of the critical state of a superconductor submitted to an increasing magnetic field.

In his book "How Nature Works–the science of Self Organized Criticality" [122], Bak gives a vivid description of the formation of a sandpile and its avalanche dynamics which can be considered a refinement of our own one given above. In his description, our sandpile is an *open system*, since we will construct the pile by adding grains of sand. The flat surface on which the sand is added represents an *equilibrium state* –energy minimum of the system–, but the intergrain friction prevents the sand from adopting this state. In spite of this, the grains start to form a pile. In the first stages, they just "stick" to the grains they have landed on. When the pile gets steeper, the grains start to topple from the landing locations to lower levels, but still provoking just *local* avalanches. The toppling events make the system *dissipative*, since heat is released due to friction. There is a moment, though, in which the average number of grains added to the pile matches that abandoning the pile off the edges, i.e., the system has reached a *stationary state*. This state is *critical* in the sense that it can be only maintained if the different parts of the pile are able to "communicate" by means of *many sized avalanches*, which eventually can span the whole pile...a fact that could not be foretold from the properties of the individual grains! *But the key feature that makes this system a paradigm of Self Organized Criticality is that a critical state "self-organizes" in the sense that it is reached with no regard of the details of the specific experiment, such as the shape of the grains or the roughness of the horizontal surface.* At least for the case of *theoretical* piles.

In fact, Bak and coworkers demonstrated in 1987 that, for a simple computational model representing the dynamics of a sandpile the following *power laws* described the avalanche size distribution:

$$P(s) \sim s^{-\tau} \tag{24}$$

and the avalanche lifetime distribution:

$$P(t) \sim t^{-\alpha} \tag{25}$$

where s and t are the avalanche sizes and lifetimes, respectively. This means that many-sized avalanches occurred in the system. Even when we are not going to describe the model in detail for the sake of brevity, it is worth noting that *all* the avalanches are considered, and not only those associated to grains falling off the edge, and that inertial effects are not taken into account. In the case of 2D piles, Bak and coworkers found $\tau \approx 0.98$ and $\alpha \approx 0.42$, respectively. A remarkable early attempt to probe the *universality* of these exponents (i.e., their robustness when the details of the simulation are changed) was sonly published by Kadanoff and coworkers [123]. From his work, one may infer that 2D sandpile models tend to show SOC behavior, but 1D models do not.

The noise spectrum associated to a lifetime distribution given by equation 25 can be calculated as $S(\omega) \sim \omega^{-2+\alpha}$. This led the authors to propose SOC as the dynamical explanation of the "$1/f$

noise" observed in many natural phenomena.

An important issue both in simulations and in real experiments with sandpiles is the problem of the *finiteness* of the system. This results in the departure from the power laws in the big avalanche region, also called "cutoff". One could test if a finite system is critical by measuring the avalanche distribution for different system sizes, and check if the different distributions collapse into a single curve when applying to the data a *critical size scaling ansatz* such as:

$$P(s,L) = L^{-\beta} f(s/L^{-\nu}) \tag{26}$$

where L is the size of the system, f is the *scaling function* and β and ν are critical exponents [124].

The explicit urging for experiments by Bak and coworkers in 1987 [116] managed to bring real sand into the laboratories. The "avalanche" started with the "rotating drum" experiment [119], which didn't show power law avalanche distributions – neither resembled too much the original sandpile model– and continued with the work of Held and coworkers on real sand 2D piles to which grains were slowly added on top [125]. Although finding power-law distributed avalanches in a certain range, they observed large avalanches causing oscillations of the slope of the pile. As pointed out in [122], this experiments still had an important difference with the original SOC model: only the off-the-edge avalanches were recorded. The existence of inertial effects in real sandpiles was a second major difference with the very simple origial model. After several other experimental studies [126,127,128,129,130,131]

an important experimental improvement was made in 1996 by the "Oslo group" [132,133], when measuring *also the internal avalanches* of slowly-driven cuasi-1D ricepiles with the help of a video camera. For elongated rice grains –i.e., when the frictional inter-grain forces suppressed the inertial effects– SOC behavior was found.

Figure 11 shows the finite size scaling of their data. The dependence on the grain shape –a detail of the system– on the SOC behavior, though, indicates that the sandpile model is not as robust as initially supposed. The off-the-edge avalanche behavior of 1D piles of balls studied by our group suggest that SOC may also depend on the *nature* of the *base* of the piles in such a way that bases which induce "ordered" profile doesn't pass the finite size scaling test, while those with bases inducing "disordered" profiles do. Figure 12 displays two extreme cases of this behavior: in the upper half, bases provoking a smooth pile profile give "uncollapsable" avalanche size distributions for three different base lengths. In the lower half, a base provoking a very disordered profile gives a nice collapse when the ansatz (26) is applied to the avalanche distributions for three different base lengths. This result is most intriguing, considering that inertial effects are not purposedly suppressed in our experiment [118].

It is not strange, then, that the next step was to look for SOC on a physical system basically analogous to sandpiles, but free –at least in a much bigger extent than sandpiles– of inertial effects: *the critical state of type II superconductors.*

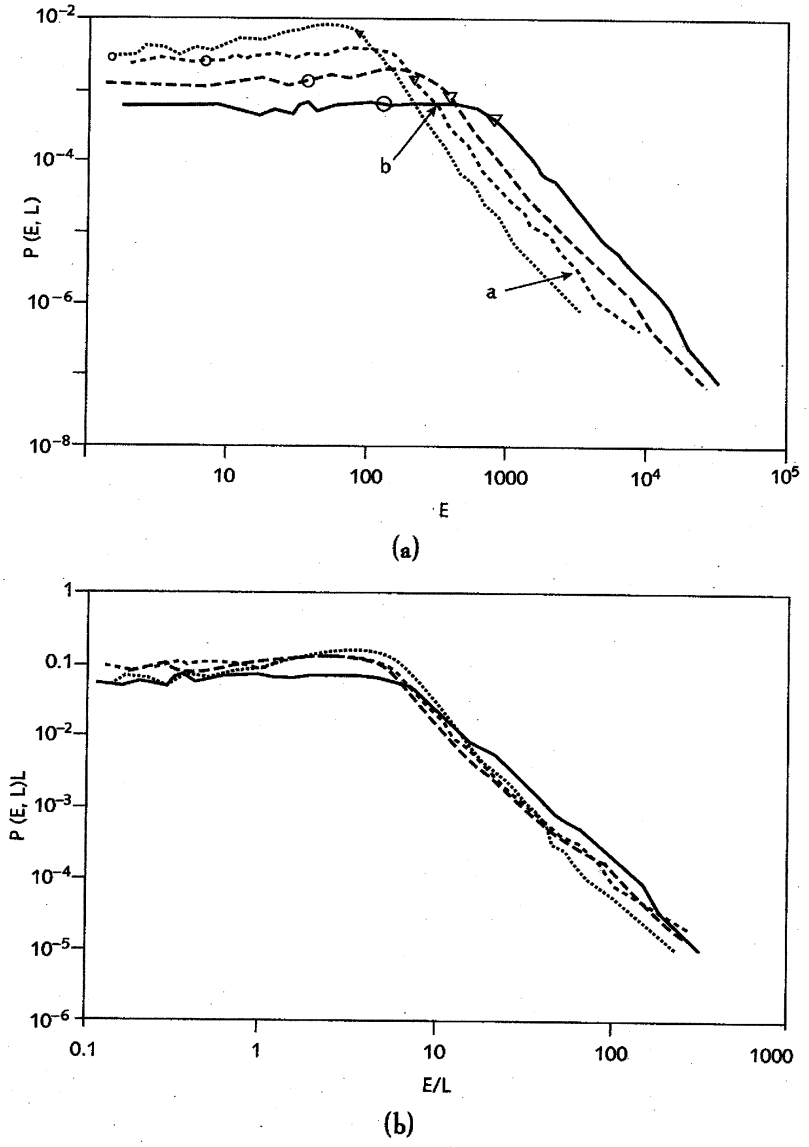

Figure 11: (a) Avalanche energy distributions for four base sizes in a ricepile, after Frette and coworkers [132]. (b) Data collapse after applying a finite size scaling ansatz [132].

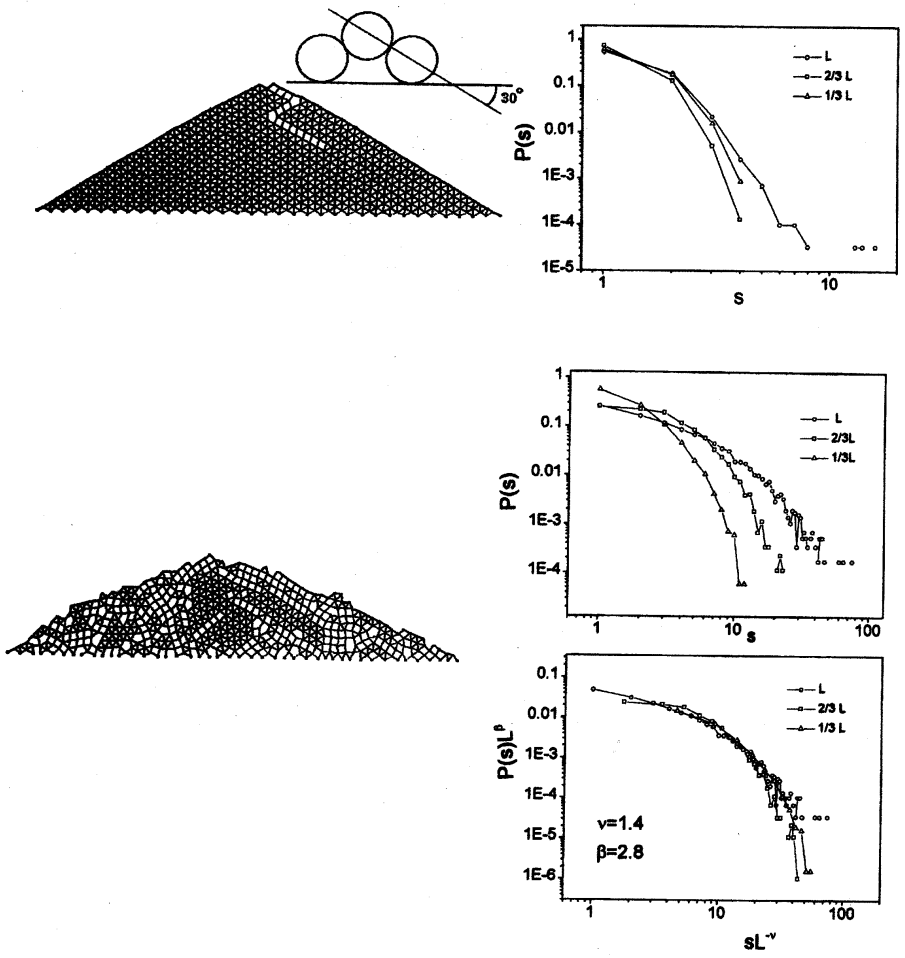

Figure 12: Base-dependent avalanche behavior in 1D piles of balls. Upper part: well ordered piles (left) produced by a conveniently calculated base show avalanche size distributions (right) which do not collapse when trying finite size scaling. Lower part: disordered piles associated to disordered bases (left) show good collapse of the avalanche size distributions measured for different base lengths (right).

4. Avalanches in the vortex state

Experiments: present and future

Field et al succeeded in 1995 in the first conscious experiment to directly establish the analogy between sand and vortex avalanches [52]. They used a setup basically similar to those previously used in references [134,135,136]: a 1800 turn pickup coil was coaxially set into a thin-walled tube of the low temperature superconductor $Nb_{0.47wt}Ti_{0.53wt}$ with 6mm of outer diameter, 0.25mm wall thickness and 3.4 mm length. Following the authors, *this geometry guaranteed a close analogy to [conical] sandpiles*. An external magnetic field was applied along z-axis with different ramp speeds, and the voltage induced at the pickup coil amplified, and recorded by a computer. The equivalent sandpile analog of this setup would be an horizontal ring with a vertical cylindrical wall along its outer perimeter, and no wall along the inner one. The sand would be continually added along the perimeter of the wall from the outside. Then, after establishing a critical profile, avalanches would start to drop across the inner perimeter of the ring. The basic idea of Field's experiment was to detect the equivalent vortex avalanches by means of the pick up coil. Then, if a "flux avalanche" of length l "drops" inside the cylinder, it will induce a voltage on n turns of the pick up coil, were $n = \frac{l}{L}N$ (L being the length of the pick up coil and N the total number of turns). Then, the detected voltage will be

$$V = \frac{l}{L} N \frac{d\phi_{actual}}{dt} \tag{27}$$

Field and coworkers defined their avalanche size as an "effective bundle volume" given by

$$s \approx l\phi_{actual} = \frac{L}{N} \int V dt \tag{28}$$

which is a convenient definition in view of the fact that it was not possible to determine l from the available data. In the 1968 experiment by Heiden and Rochlin, a $1 - mm$ coil was used but, even in that case, the authors expressed their preoccupation about the existence of a geometrical factor tending to increase the number of counts due to bundles linking only part of the coil [135].

Figure 13a displays the temporal response of the voltage at the pick up coil for a field window of $30Oe$ centered at $7.55kOe$ and measured at a sweep rate of $5Oe/s$ (figures b and c are horizontal enlargements of Figure 13a). Following the authors, two contributions can be identified: a flat background related to a continuous entrance of flux at the rate of the external field ramp, and *pulses related to sudden entrances of flux bundles, i.e., avalanches*. The latter are estimated to represent 3 percent of the total flux income. Although the authors calculate that the number of vortices associated to avalanches range from 50 to 5000, this is pervaded by the indetermination in the bundle length, l.

Figure 14a shows the avalanche size distributions reported in [52] For the three fields studied and $5Oe/s$ sweep rate, *they can be described by power laws* for more than one decade. This situation is not common in sandpile experiments, where a departure from the pure power-law behavior is seen [125,128,130]. Some authors interpret this situation as a consequence of the finite size of their

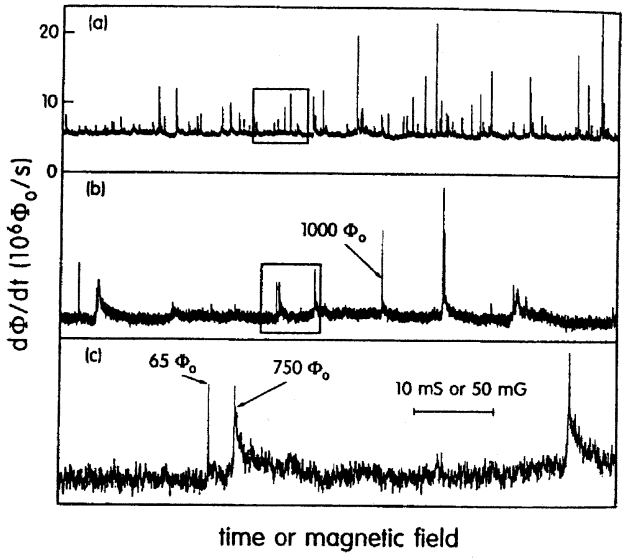

Figure 13: Response of the pick up coil of Field and coworker's experiment [52] which demonstrates the avalanche behavior of vortices in low-T_c tubes.

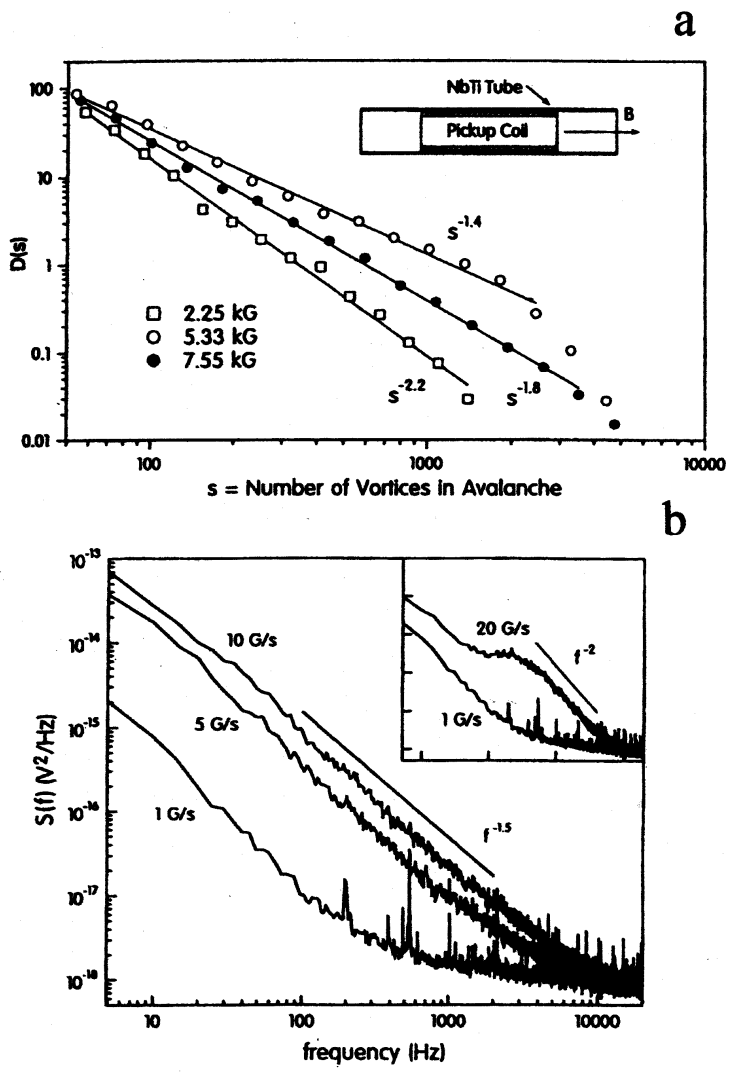

Figure 14: (a) Avalanche size distributions in the experiment of Field and coworkers [52] for different field windows. (b) Avalanche power spectrum reported by the same authors.

systems, which is not a very important handicap in the vortex avalanches here described, since, following [52], the number of vortices in the wall is typically a million times greater than those involved in avalanche events). The authors didn't find the relaxation oscillator behavior observed by others in 2D sandpiles [125] which is related by them to the lack of inertial effects in vortices. As mentioned earlier, this situation makes vortex dynamics closer to sandpile models [116,123]. The observed variation of the power law exponents with the applied field in the range from -1.4 to -2.2 is explained in [52] to the different inter-vortex and inter-pin distances attained at the different field values. This may be considered reminiscent of the influence of grains friction, shape [132] or even of the type of base [118] on analogous exponents in the case of sandpile dynamics. Finally, the authors report the power spectrum of the observed avalanches, defined as the squared Fourier transform of a field sweep similar to that of Figure 14b. While a $1/f$ behavior is seen for slow ramps, a faster ones give a Lorentzian peak, and a $1/f^2$ spectrum at high frequencies. The authors conclude from this fact that the critical behavior is achieved only very near the marginally stable state, when the system is slowly driven (typically $5Oe/s$ in their experiments). Interestingly enough, Heiden and Rochlin found *exponential* distributions of "flux jumps" entering their cylinder independently from the field sweep rate, at least in the range from 10 to $100Oe/s$ in their 1968' pioneering experiment [135]. Even when their "flux jumps" distributions included a higher number of events than those presented in figure 14a, the exponential behaviour was found for less than a decade, and the authors believed that their statistics was still poor for the assessment of the exponential behavior.

Let us turn back to the problem of the "avalanching" flux bundle length. One could estimate this length using the theory of Collective Pinning [137,138]. By treating the vortex lattice plus random pinning as an elastic system , this theory assumes that vortices elastically deform to "accommodate" to a distribution of pinning centers *within a characteristic pinning length along* z roughly given by [139,140]:

$$\mathrm{L}_c \approx \xi \sqrt{\frac{J_0}{J_c}} \tag{29}$$

where J_c and J_0 are the measured and the depairing critical current densities, respectively, and ξ is the coherence length. These vortex segments –or vortex bundle segments, at higher fields– are the "objects" which may "jump" to a neighbor metastable state within Collective Pinning Theory [139]. If we substitute typical values of these parameters for a low-T_c superconducting alloy at temperatures under $5K$ [43] ,*we get a correlation length of the order of a few microns.* When considering very poorly pinned materials –i.e., very small J_c– the correlation length increases to tenths of a millimeter. Is that the typical *avalanche* z-axis bundle length in the experiment of references [52,135]?

In our opinion, revisiting the 1965' experimental set up of Wischmeyer [136] would be a fruitful exersise to get, at least, an approximate response to that question, and, generally speaking, more insight into Field and coworkers' experiment. It also consisted in a low-T_c cylinder submitted to an axial magnetic field , but *three* detection coils were coaxially mounted, as depicted in the lower

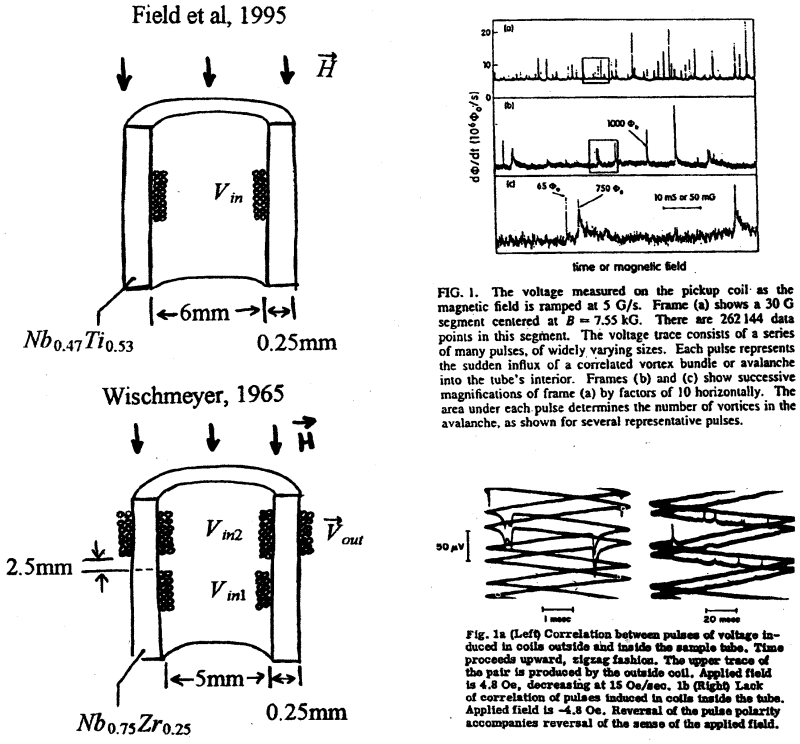

FIG. 1. The voltage measured on the pickup coil as the magnetic field is ramped at 5 G/s. Frame (a) shows a 30 G segment centered at $B = 7.55$ kG. There are 262 144 data points in this segment. The voltage trace consists of a series of many pulses, of widely varying sizes. Each pulse represents the sudden influx of a correlated vortex bundle or avalanche into the tube's interior. Frames (b) and (c) show successive magnifications of frame (a) by factors of 10 horizontally. The area under each pulse determines the number of vortices in the avalanche, as shown for several representative pulses.

Fig. 1a (Left) Correlation between pulses of voltage induced in coils outside and inside the sample tube. Time proceeds upward, zigzag fashion. The upper trace of the pair is produced by the outside coil. Applied field is 4.8 Oe, decreasing at 15 Oe/sec. 1b (Right) Lack of correlation of pulses induced in coils inside the tube. Applied field is -4.8 Oe. Reversal of the pulse polarity accompanies reversal of the sense of the applied field.

Figure 15: Upper section: set-up by Field and coworkers (left), and resulting pickup voltage (right) [52]. Lower section: set-up by Wischmeyer (left), and resulting voltages at the three pickups involved in the experiment [136] .

left section of Figure 15. Two of them were located at the inner wall of the cylinder in such a way that their adjacent ends were a distance $d = 2.5mm$ apart, and the third at its outer wall. The lower right section of Figure 15 shows measurements obtained by Wischmeyer with his set up which are roughly equivalent to those depicted in the upper right section of Figure 15, except that *three* signals are detected. While the temporal evolution of the voltage of the coils inside and outside the tube are highly correlated, the signals corresponding to the coils into the cylinder are poorly correlated.

Winschmeyer results indicate that not only the flux exit through the cylinder wall, but even the flux entry, may be characterized by peak events!. This can be understood for system-spanning avalanches –a big exit of vortices off the edge implies a decrease of vortex density at the entry– or even for avalanches occurring close to the entry boundary. But if it happens to *all* the avalanches, it means that some kind of surface barrier prevents the applied field to *enter* the system smoothly. The data from [136] is not good enough to discern among these possibilities. They also give a clue about the length of Field's avalanching objects: a few millimiters seems to be its upper limit (definitively 2.5 mm in [136]). Let us imagine an experiment with Winschmeyer's setup in which the distance d can be diminished until correlation between the pulses detected by the two inner coils is observed. The corresponding value of d can be interpreted as the *maximum length* of the bundles crossing the wall. A statistical analysis of these correlations for even smaller distances could even give an idea of the distribution of flux bundles lengths in the z-direction and then, would allow us to learn more about the *flux* sizes of the avalanches. We even can learn how to control the size of the avalanching objects (related to vortex "rigidity" [43] by tuning the measuring temperature. Of course, if expression 30 gives a true estimation of the avalanching bundles' length, this experiment would never detect correlation between the outputs of the inner coils, at least for the d values reasonably affordable in the experiment.

As can be induced from the last paragraph, besides inertia, *temperature* is another important difference between the avalanche behavior of superconductors and of sandpiles. In general, avalanche experiments on sandpiles are not performed in the presence of mechanical vibrations. So, a perfectly equivalent experiment on superconductors should be performed *at zero Kelvin*. Although it is not possible, common sense indicates that the avalanche behavior of superconductors would approach that of sandpiles only at very low temperatures. But this happens not to be the case, as demonstrated by the experiments of Zieve et al [53], Nowak et al [54], and Behnia et al [58].

The 1996's report of Zieve and coworkers [53] used two experimental novelties in the study of vortex avalanches: state-of-the-art magnetic field sensors, and High T_c materials [‡] The former consisted in the use of photolithographically prepared miniature Hall probes to detect the magnetic induction very close to the sample. This technique had been gaining popularity among the superconducting experimental community in the nineties [142,143,144,145,146,147,148,149].

[‡]The first observation of vortex avalanches using a similar setup was reported in 1993 by Seidler and coworkers [50]. We instead discuss in detail reference [53], since it can be regarded as a continuation of [50] with a heavy accent on the dynamical origin of the avalanches and their sandpile analogy, as we will see.

Zieve and coworkers studied untwinned $YBa_2Cu_3O_{7-\delta}$ single crystals with a critical temperature of 92 K. They ramped an external field applied parallel to the smaller dimension of the crystals, and measured the *internal* avalanches on the samples by mounting them on a miniature Hall probe with a typical active area of $3\,\mu m \times 5\,\mu m$. This resulted in a sensitivity of a single flux quantum, a dramatic improvement as compared with Field and coworkers' experiment [52]. Another interesting feature of the micro Hall probes is that they allowed the measurement of "internal" avalanches –which can be compared with the rice piles experiments reported in [132]– in contrast with the off-the-edge vortex avalanches reported before [52]. Following the authors, the results were basically similar when the sensor was positioned at different spots on the crystal surface, of typical dimensions of $1.05 \times 0.5 \times 0.005\,mm^3$. The avalanche dynamics was explored at *very low* temperatures ($0.1\,K - 0.4\,K$, approximately), and hysteretic effects were studied by ramping the external magnetic field from zero to around $80\,kOe$, and then back to zero, at a sweep rate of $7\,Oe/s$.

Even when Zieve and coworkers' experiment eventually introduced demagnetization artifacts, their geometry allowed –in principle– a better control of the z-axis length of the avalanching objects than in cylinder experiments. Let us estimate L_c in their experiment with the help of formula 30. We first calculate the depairing critical current for a typical YBCO crystal with the magnetic field applied along the c-axis at $0K$ by substituting $\xi_{ab} = 30$ and $\lambda_{ab} = 3nm$ in the following Ginzburg-Landau result [17]:

$$J_0 = \frac{\Phi_0}{3\sqrt{3}\pi\mu_0\lambda^2\xi} \tag{30}$$

which gives $J_0 \approx 3.6 \times 10^{11} A/cm^2$. A rough estimate of J_c based on the hysteresis loop reported in [53] (upper section of Figure 16) and the crystal dimensions also reported in [53] gives a lower limit for J_c of $10^6 A/cm^2$, a value typically reported for YBCO crystals form magnetic measurements (see, for example, reference [90]). If we substitute this value and J_0 in formula (30), we can estimate an upper limit of of $20\mu m$ for L_c, *which is bigger than the reported crystal thickness of* $5\mu m$. This is a good point in favor of Zieve and coworkers experiment [53]. Besides the crystal thickness, a second relevant length related to vortex dimensionality appears in the case of any layered superconductor: the interlayer spacing. As pointed out in section 2.1, this situation provokes the appearance of "pancake" vortices on the superconducting layers. While for low enough temperatures and fields these vortices are strongly correlated as 3D strings, (which can be treated as "conventional" vortices), above a certain line in the H-T plane the correlation can be broken, and the 2D pancakes move independently [140]. *This complicates the dynamics for any experiment to detect vortex avalanches on High T_c superconductors, unless we make sure to work in the "vortex lattice" or "vortex glass" regions of the phase diagrams depicted at the lower section of Figure 1.* This condition seems to be also fulfilled in [53] due to their very low temperature window.

A conceptually simple experiment would help to get rid of any doubt about the dimensionality of the avalanching objects for any geometry involving a magnetic field perpendicular to a super-

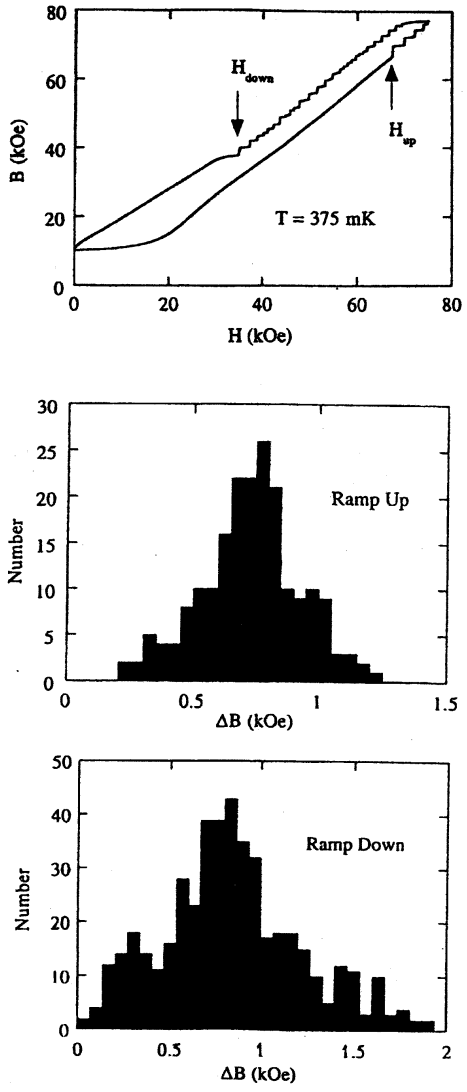

Figure 16: Top graph: Typical hysteresis loop measured by Zieve and coworkers [53] on a YBCO crystal in which steps corresponding to vortex avalanches are visible. Intermediate and lower graphs: avalanche sizes distributions derived from the up and down field ramps in the same experiment [53].

conducting crystal or foil: it would consist in attaching not one, but *a couple of paralell micro Hall probes situated at the two wide surfaces of the YBCO crystal* and analyze the *synchronism* of the vortex avalanches measured by either probe. This experiment can be regarded as the "magnetic relative" of the six-terminal flux transformer set-ups that has been used for studying different vortex phase transformations through I-V curves in HT_c superconductors [150,151,152,153,154,155,156,157]. From the instrumental point of view, it is definitively closer to the experiment by Lee and coworkers [158]. They measured magnetic flux noise at opposite sides of YBCO and BSCCO crystals and films in the thickness range between 0.075 and 30 microns *with two SQUID's*. The authors concluded that the correlation of vortex motion at both sides of the sample depends on its thermomagnetic history and pinning details. Their experiment has two important differences with the one with micro-Hall probes. Firstly, while the latter is "local" ($10 \times 10 \mu m^2$), the former is "global" ($180 \times 180 \mu m^2$ SQUID hole area). Secondly, the latter measures the vortex movement correlation associated to a field ramp, while the former probes the thermally activated flux motion it *in time* at zero field.

The upper graph of figure 16 contains some of the most interesting findings reported in [53]. First, vortex avalanches are observed as steps when the magnetic field is ramped up and down. Second, they appear at a certain field value, H_{up}, and disappear at a *different* value, H_{down}, which are independent from the field ramp rate. H_{down} showed to be particularly stable against variations of the temperature and field ramp histories. The results of several well conceived experiments made the authors reach the conclusion that *the difference between H_{up} and H_{down} ,i.e., between the ramp directions, is an intrinsic property of the system than cannot be "suppressed" by changing the experimental conditions*. The second major finding of Zieve and coworkers is that the avalanche size distributions in both ramp directions are not power-laws, but sharply peaked, and centered around 750 flux quanta (see the two lower graphs in Figure 16). This doesn't fit into the SOC scheme.

These distributions could be expected from thermally triggered flux jumps, as described in section 2.2.2. However, the authors dissipate such doubts with several arguments. For instance, their avalanches are observed in the "high" field region, while thermally triggered flux jumps are typical of the "low" field region, and their steps never reach the line $B = H$ –i.e., the magnetization never vanishes– which constitutes a common "catastrophe" in thermally triggered flux jumps. They also do not depend too much on field rates, as expected for thermal instabilities.

Then, the authors conclude that their avalanches have a true *dynamic* origin, and try to give an intuitive picture of the observed hysteretical behavior through the sandpile analogy. As described in section 3, the mechanical process to fill a box with sand to get the "V-shaped" Bean's profile is different form that required to resemble the decreasing-field Bean's profile: while in the former, sand should be *added* through the boundaries at the *higher* positions of the pile, in the latter it must be *removed* from the *lowest* positions. These two processes are quite different, since the lower positions support much of the overall pile weight, so sand removal may trigger avalanches easier

(corresponding to the lower values of H_{down} as compared to H_{up}) [§] Zieve and coworkers extend the analogy to account also for the peaked avalanche distributions observed: in their opinion, vortex mass renormalization [140] takes place at the very low temperatures of their experiments, making vortex inertial effects significant. This brings closer their vortex system to sandpiles, which, as stated in section 3, have been found to show peaked avalanche size distributions due to inertial effects [125,128].

Nowak et al [54] performed a variation of Field and coworkers' experiment, but substituting the superconducting cylinder by Nb rings with inner and outer diameters of $15\mu m$ and $98\mu m$, respectively, and $0.5\mu m$-thickness. They used the same system as [53] for avalanche detection: one $3\mu m \times 5\mu m$-area Hall probe was positioned at the center of the hole, and a second one, $22\mu m$ off-center and directly above the ring. The sensitivity of these probes were $10\Phi_0$ and Φ_0, respectively. They allowed the measurement of the *total* flux involved in avalanches crossing the perimeter of the hole, and also those occurring *a certain position* above the superconducting ring (internal avalanches). This geometry might allow to approach the vorticial analogy to a *typical* sandpile, i.e., that excited by adding particles at the top of the pile. To do it, we just need to increase the magnetic field *only at the hole*. This can be achieved by using a miniature split ring-solenoid fitting closely over the specimen at the hole region. Internal and off-the-edge avalanches could be measured by placing Hall probes on the ring and at its outer perimeter, respectively.

Nowak and coworker's geometry allows –in principle– to control of the z-axis length of the "avalanching" objects even better than in the case of [53], since no layered structure is present in Nb. Let us estimate L_c in this experiment. We first calculate the depairing critical current for pure Nb at $0K$ by substituting $\xi = 40nm$ and $\lambda = 85nm$ [141] in 31, which gives $J_0 \approx 3.4 \times 10^7 A/cm^2$. Substituting in formula (30) this and the value $J_c = 5 \times 10^{10} A/m^2$ reported in [54] for their Nb films, gives $L_c \approx 0.1\mu m$. Although this is twice the film thickness use for fabricating the rings, this proportion might be even lower, since J_0 may be smaller than that calculated from 31, due to impurities in Nb [160]. Then, a "worse" Nb material from the point of view of pinning strength would be convenient in this experiment to *guarantee* "avalanching objects" of the same length of the film thickness. As a matter of fact, this can be easily achieved for thin-film amorphous superconductors [161].

Figure 17 shows some of the basic findings of Nowak and coworkers [54]. As in the case of [53], steps appear in the $B - H$ plane, indicating the occurrence of avalanches at different temperatures –always higher than those studied in [53]–. Interestingly enough, no trace of H_{up} and H_{down} fields similar to those reported in [53] is observed. This might be related to the much lower field values in the present experiment. The most interesting fact observed by Nowak and coworkers is the dramatic dependence of their avalanche size distributions with temperature, as summarized in Figure 18. Below $T/T_c > 0.35$, the avalanche size distribution follows a decreasing exponential,

[§] To the author's knowledge, no experiment or has been conducted to check out such as important hysteretical behavior in sandpiles. Although not aimed at exploring hysteresis, recent *simulations* of Manna and Khakdhar [159] indicate power-law avalanche distributions for internal avalanches in granular media where the grains are *removed* from the bottom of a 1D pile. No inertial effects were considered.

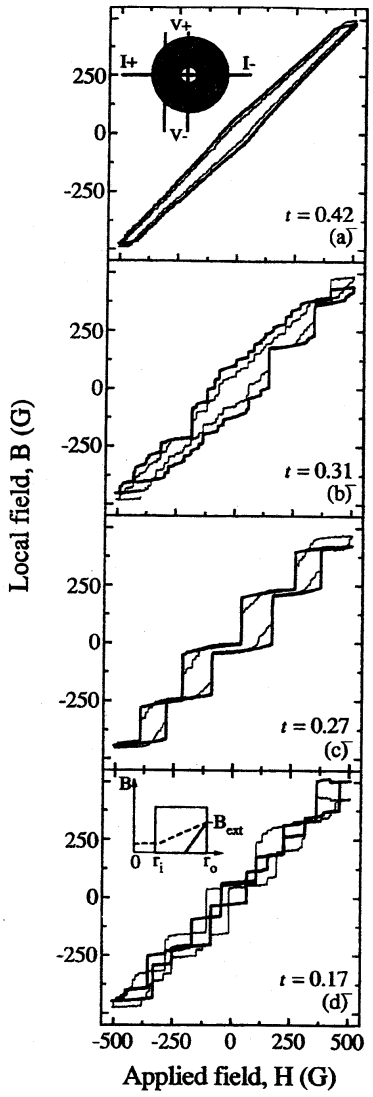

Figure 17: Hysteresis loops measured by Nowak and coworkers [54] on a Nb ring (depicted as an inset in the top graph) in which T-dependent steps representing vortex avalanches are visible ($t = T/T_c$).

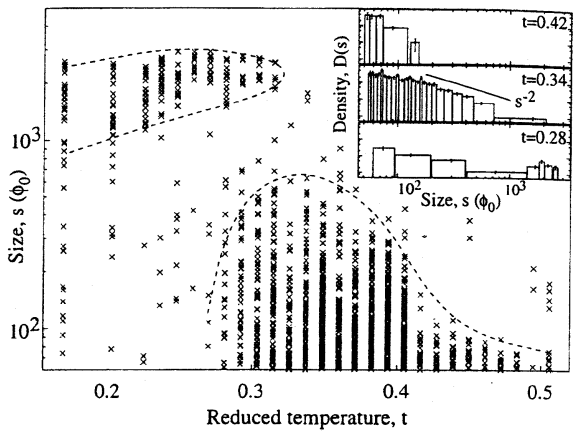

Figure 18: Representation of the avalanche statistics as measured by Nowak and coworkers, extracted from [54] .

as reported in [135], and the avalanches are not "complete" (they don't reach the $H - B$ line). For $0.2 < T/T_c < 0.3$, however, it is sharply peaked around $2000\Phi_0$. The corresponding avalanches are system-spanning and "complete", which suggests thermally-triggered flux jumps. For $0.2 > T/T_c$, a broad avalanche size distribution is recovered, but it is not exponential. These observations remained the same within a ramp rate window from 2 mOe/s to 20 Oe/s, indicating that the experiments took place in the slowly driven regime.

The authors explain their data on the basis of a thermally triggered mechanism typical of flux jumps. They even define a thermal stability parameter (see section 2.2.2), for their ring geometry, and argue that the broad distribution of avalanches they observe in the range $0.3 < T/T_c < 0.4$ –and reported by others [52,135]– is related to a regime in which that parameter is marginally greater than 1. This contrasts with a SOC dynamic mechanism for vortex avalanches.

To the author's knowledge, the last experimental study of non-catastrophic vortex avalanches in slowly ramped external fields is the 1999' one by Behnia and coworkers [58]. Pulling even further the Hall micro-probe technique, these authors attempted to study in detail the spatial and temporal correlations of *internal* vortex avalanches in the x-y plane of a a $20\mu m - thick$ polycrystalline Nb film of lateral $0.8 \times 0.8mm^2$. The measurements were performed using a row of 8 equally spaced Hall micro-probes of $20 \times 5\mu m^2$ area each, able to detect $0.16\Phi_0$. Each row was 0.35 mm long, lying on the film perpendicularly to one of its edges, in such a way that the sensor closest to the film

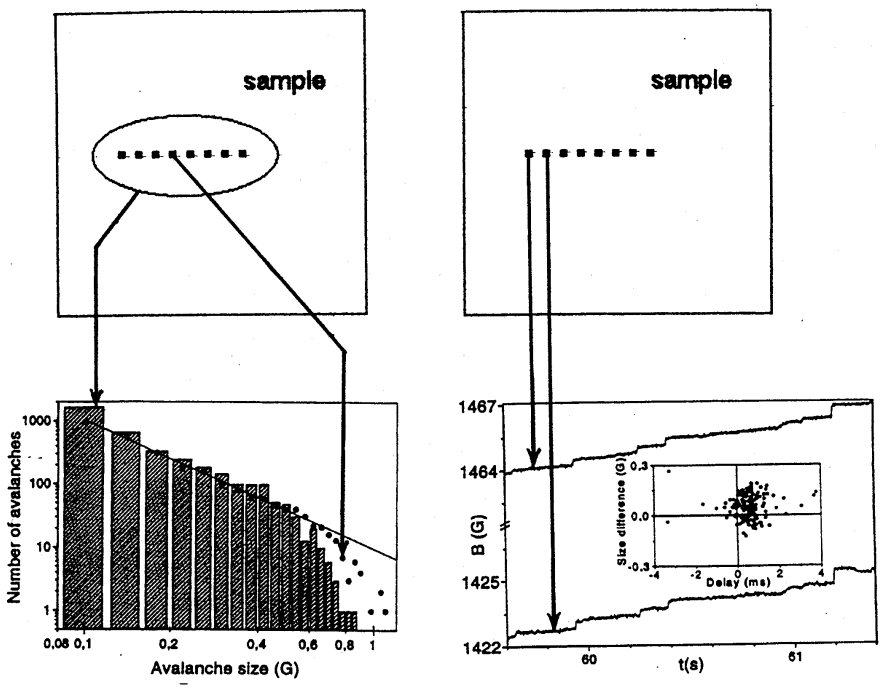

Figure 19: Avalanche size distributions (left) and spatiotemporal correlations of avalanches (right) on a Nb foil submitted to an increasing magnetic field [58].

edge was 0.2 mm away from it (see the upper section of Figure 19 for an approximate sketch of the sensors arrangement). As in previous cases, let us estimate the collective creep bundle size in this experiment, based on the available data. Considering formula (31) and the values $\xi = 60nm$ and $\lambda = 150nm$ as extracted from the values of the critical fields [162], we obtain $J_0 \approx 7 \times 10^6 A/cm^2$. A rough estimation of the critical current density at $H = 1500Oe$ based on the application of Bean's model to the $B-H$ loop reported by the authors gives a lower limit of $J_c \approx 5 \times 10^4 A/cm2$. When these values are substituted in formula (30), we get an approximate upper limit for L_c of $0.7\mu m$, which is quite smaller than the film thickness. So, the "rigidity" of vortices measured in the experiment is not guaranteed. After checking the establishment of the Bean's critical state profile at $T = 4.8K$ –something difficult to assess in previous experiments due to the small amount of Hall sensors–, Behnia and coworkers ramped up the external field at $1.1Oe/s$ starting at $B = 0.15T$. They obtained, at each sensor, a $B-H$ pattern with *steps* qualitatively similar to those reported in [53] and [54], which indicated the presence of flux avalanches. *The authors estimated that 40 to 70 % of the flux increase into the sample was in the form of avalanches and not fluidlike, which contrast with the 3 % reported by Field et al in 1995* [52].

At the lower left of Figure 19, the avalanche size statistics is displayed for one sensor (black

dots) and for the output of a whole row (columns). Both distributions follow a power law for less than a decade with a critical exponent of -2.1, within the range of those reported in [52], with the biggest avalanches comprising around 5 vortices under one probe area. However, the differences in the zone of big avalanches suggest that not all the avalanches extend through the whole length of the row (if they did, the two outputs would be exactly the same). Note that measuring the output of an entire row of sensors introduces an "artifact" qualitatively similar, within the x-y plane, to that present in reference [52] due to the extension of their pick up coil along z-axis. To further explore this finding, Behnia and coworkers analyze the spatio-temporal correlations of the avalanches measured on two micro-probes located $50\mu m$ apart, resulting in the $B-H$ diagram at the lower right of Figure 19. The avalanches at the sensor closer to the sample boundary generally occur first, and then propagate "down-the-hill" to the second sensor. They also observed that avalanches generally increased when moving in the same direction. These two facts are reflected in the right-left and up-down assymetry in the inset of the $B-H$ graph, respectively. All this findings suggest a SOC picture of the observed avalanches.

Under $T = 3.4K$, however, a completely different picture arises: catastrophic, hysteretic, avalanches with peaked size distributions are observed, in agreement with the work of Zieve and coworkers [53]. As them, Behnia and coworkers claim that such avalanches are not thermally triggered, since they demonstrated to be insensitive to the field ramp speed. They also present the $H-T$ phase diagram of their sample –a very valuable data not often reported by other authors–, and remark that the catastrophic avalanches occur in a low temperature region *close to H_{c1}, and far from H_{c2}*.

The authors suggest that, close to H_{c1}, the critical state is not well established, so, as reported for sandpiles, the occurrence of "quasi-periodical" avalanches can be related to the "absence of a single critical slope". This contrasts with our own results in 1D piles (see Figure 12) and the "Oslo model" in which SOC behavior is observed only when "dynamically disordered" pile profiles are attained [118,132,133].

A quite different approach to the measurement of vortex avalanches was used by Aegerter in 1998 [56]: *instead of ramping the external field –as in the cases previously discussed– the author measures flux avalanches during the thermally activated time relaxation of the magnetization* at different temperatures. At each temperature, the author measures the *global* magnetization of a $Bi_2Sr_2CaCu_2O_8$ crystal during a 24-hour period by means of a SQUID magnetometer, after applying a certain magnetic field to the sample in zero-field-cooling conditions. However, neither the value of the applied field nor the relative orientation of the crystal are reported in reference [56]. The avalanches appeared as *spikes* in the magnetization versus time characteristics. Even when the avalanche dynamics studied in this "thermally driven" experiment cannot be compared with those reported in "field-driven" conditions [135,52,53,54,58] in a straightforward fashion, it is worth pointing out the basic observations accounted by the author: *the avalanche size distributions are described by power laws at "low" temperatures ($0.06T_c$) and at long relaxation times, while they are fitted by exponential laws at "high" temperatures ($0.8T_c$), and at short relaxation times.* When

Ref	*Geom.*	*Material*	*Sensor*	*Avalanche type*	*Trange*	*H range [kOe]*	*Avalanche distribution*
[135] (1968)	hollow cylinder	Pb-In	pickup coil	off-edge	0.6 T_c	0.550 - 0.850	exponential
[52] (1995)	hollow cylinder	Nb-Ti	pickup coil	off-edge	0.3 T_c	2.25 - 7.55	power law (slow ramps)
[53] (1996)	planar	YBCO crystal	Hall probe	internal	T $\leq$ 0.01 T_c	0-80	peaked
[54] (1997)	ring	Nb film	Hall probes	off-edge & internal	0.15 1.12 T_c-	-500 - 500	peaked/pow. law (dep. on T)
[56] (1998)	planar	BSCCO crystal	SQUID	off-edge	0.06- 0.8T_c	?	exp/pow. law (dep. on T & t)
[58] (1999)	planar	Nb film	Hall probes	internal	0.52 T_c	1.5	peaked/pow. law (dep. on H & T)

Table 1: Basic features and results of experiments on vortex avalanches discussed in the text, as extracted directly or indirectly from the respective references. Most of the experiments were performed by ramping the external field in the range from 0.002 to 100 Oe/s, except for [56], in which the field was not ramped.

power laws arise, the author obtains an exponent of 2 in their avalanche distributions, very similar to that reported in [52] from global, field-driven experiments at $0.3T_c$. An interesting additon to Aegerter's experiments would be to detect "thermally activated" avalanches in the temperature region $T < 0.01T_c$ and check if the peaked avalanche distributions reported by Zieve and coworkers in their field-driven experiments on other high-T_c, YBCO, appear here.

Some of the experiemntal details and results reported in the avalanche-detection experiments discussed above, have been summarized in Table 1. Although their contents might be partially unnacurate –due to lack of space and difficulties in finding data in some of the articles cited– it brings a necessary global idea of the current "state of the art" in the subject. It makes clear, for example, that many voids have to be filled up to get a complete picture of the avalanche dynamics in superconductors. It may be suggested, for example, that the micro-Hall probe technique should be used to explore more thoroughly the H-T diagram of the different materials in the search of avalanche dynamics. Even when most of the cited papers are fine pieces of experimental work, they do not spot the detected dynamic regimes in the context of the H-T diagram for their specific sample. On the other hand, some experimental details not reflected directly in Table 1 also present voids. For example, the time windows explored by the different authors for estabishing their avalanche size distribution data roughly vary form a hundred seconds in [52] and [58] to several hours in [53] and [54].

Doughnut-vortex avalanches

Let us examine the experiment depicted in Figure 20: a straight current-carrying wire is located along the symmetry axis of a type II superconducting hollow cylinder with pinning. Due to the azimuthal magnetic field created by the wire, an asymmetric critical state is established on the crossection of the cylindrical shell associated to a distribution of doughnut-shaped vortices like

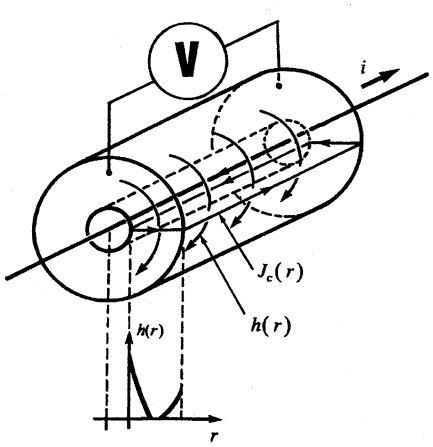

Figure 20: Type II superconducting hollow cylinder with a coaxial current-carrying wire: critical state of "doughnut-shaped" vortices [25] .

those described in section 2.1 [25]. This asymetry is connected to the fact that the wire-associated "external" field in which the cylinder wall is embedded is higher at the inner wall, and lower at the outer wall. Let us now suppose that we *slowly increase* the current on the wire.

By analogy with experiments and simulations on slab geometry in which the external field is ramped, vortex avalanches are likely to occur. In principle, their fingerprint would be *spikes* in the longitudinal voltage of the cylinder, which would eventually resemble those depicted in Figure 13. It doesn't seem to exist a trivial "sandpile" analogy of this experiment in which the avalanching objects change their length –and, following formula 8, their electromagnetic energy– as they move. Is this system expected to show SOC?.

A final divertimento: "Magnetic" and "Superconducting" earthquakes

Earthquakes are clearly one of the natural catastrophes calling for a sound physical model able to yield predictions as accurate as possible. Even though earthquakes are enormously complex phenomena involving the dynamics of disparate elements ranging from the Earth's crust to human constructions, there is one fact that makes it reasonable to tackle the problem: earthquake intensity distributions measured along many years in different regions follow a simple power law known as *Gutenberg-Richter law* [163].

Burridge and Knopoff [164] introduced a spring-block model for earthquakes basically similar to that represented in Figure 21. In the model, a tectonic fault is represented by a two-dimensional

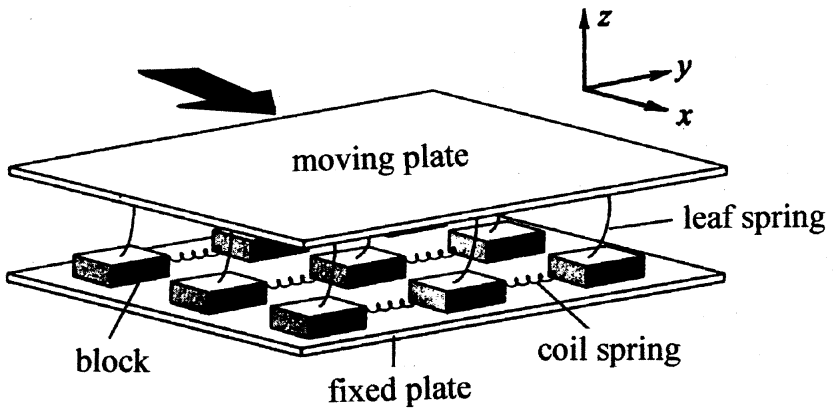

Figure 21: Block-spring model for earthquakes [122].

array of blocks resting on a surface with friction. The blocks are interconnected by coil springs along the y-axis, and each one is linked to a moving plate through leaf springs, which account for the forces on the material near the fault due to tectonic plate motion. When the plate is moved along x-axis, no block moves until, at least, one of them receives a force from its leaf spring higher than a certain threshold. When this happens, the block slips in the x-direction, which increases the forces on the neighboring blocks via the coil springs, which eventually induces a "chain reaction" resulting in the displacement of several blocks. In the model, this *avalanche-like* event is identified as an earthquake, whose intensity can be defined as the total displacement of the blocks. Simulations show that the distribution of the avalanches in such model follows a power law, even when dissipation is considered (i.e., part of the elastic force is not transmitted to the neighboring blocks). This has been interpreted by many authors as a demonstration that earthquakes display SOC behavior [165,166,167,168,122]. Even more, the finite size scaling analysis of this model indicates that it belongs to the same universality class exhibited by one-dimensional granular piles [133] and interface deppining [169]. Similar results have been found when the model was translated into a mechanical experiment [170]. Interestingly enough, when inertial effects are considered (i.e., the slips events are not instantaneous), simulations indicated that power laws are only obtained for "small" earthquakes, but more or less periodic "big" earthquakes take place [171], which resembles better the rotating drum experiments with sand of reference [119] than real earthquakes.

A curious variation of the earthquake model would be to substitute the springs by magnetic forces. This can be achieved by means of the experimental setup depicted in Figure 22: a regular set "primary" permanent magnets are stuck to the upper face of a nonmagnetic slab which rests on a second plate. A second set of magnets is situated on the lower face of the latter, in such a way that they are kept in position through the attractive interaction with the "primary" set

of magnets along the x-axis (the magnetic moments of both layers of magnets are in the same direction). Besides this interaction, the "secondary" magnets experience a repulsive magnetic interaction among them in the x-y plane. These interactions along z-axis and along the x-y plane play the role of the forces exerted by the leaf and coil springs of the earthquake model depicted in Figure 21 (although a perfect analogue would require coil springs also along x). The difference would basically rely in the details of the forces involved, particularly their *long range* nature, which contrasts with the short range commonly assumed. Now, we start to move the upper plate. Since the "secondary" magnets are submitted to a frictional force against the lower acrylic plate, avalanches can appear when the magnetic force exerted on one of these magnets surpasses the frictional threshold. The present author has performed some preliminary measurements with a very limited amount of magnets in this schedule, and slip events spanning two orders of magnitude in are easily achieved. The displacements of the secondary magnets can be measured by analyzing images recorded by a CCD camera or, even better, using highly-linear, contactless capacitive sensors. Would this system show SOC, or it will be suppressed by the nature of the magnetic forces and the strong inertia of the magnets?

We have purposely represented in Figure 22 not a squared, but an hexagonal arrangement of "primary" magnets. In fact, this set-up has many points of contact with a system of superconducting vortices piercing a pair of paralell superconducting films separated by an insulating layer, a system studied by Ivar Giaever in his elegant 1966' "flux transformer" experiments [172], in which a transport current is applied to the "primary" superconducting film, and a the voltage drop is measured along the same direction on the "secondary" film. In this system, the field- and temperature-dependent vortex-vortex interactions in the x-y plane described by formula (10) would match the coil springs in the earthquake model, while the elastic moduli for the triangular vortex lattice c_{44} (tilt) and c_{66} (shear) – which are also functions of B and T [173,174,43,140]– would account for the leaf spring action. This means that a careful tuning of the applied field and temperature would allow to scan a continuum of "spring" characteristics. In our experiment, the transport current on the "primary" film would be ramped up at a certain rate, and the time integral of the voltage measured on the "secondary" film would give the eventual flux-avalanche behavior, in a way somewhat similar to that of the 1995' experiment by Field et al [52]. A computational model for this experiment will be drafted in the next section.

Our magnet experiment can be further enriched by including several layers of nonmagnetic plates with "secondary" magnets, and measure the resulting avalanches, for example, at the bottom layer. This would mimic the situation of a high T_c crystal with a magnetic field applied perpendicular to the ab planes of the structure: the magnets correspond to the "pancake" vortices introduced in section 2.1, provided we were working in a region of the H-V phase diagram were the pancake vortices have lost their Josephson coupling, and only the magnetic interaction remains. It should be underlined, though, that a more complex elastic theory of the flux line lattice is needed to describe such system [140].

Modern techniques allowing the fabrication of normal metal, semiconductor and supercon-

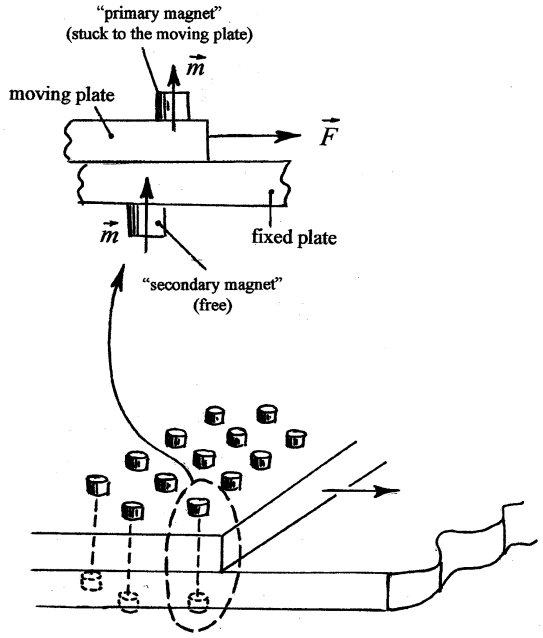

Figure 22: "Magnetic earthquakes": a variation of the mechanical earthquake model depicted in Figure 20 proposed by the author.

ductor micro- and nano-structures invite to expand further our analogies. For example, two-dimensional arrangements of islands of Al in the normal state interconnected by tunnelling junctions in the x-y plane and capacitively coupled between them and to a ground plane [175,176,177] give another reasonably good analogy with the earthquake model. Typical experiments involving these arrangements is the measure of I-V curves when the arrangement is excited by a voltage, provoking transport of charge from island to island, through tunnelling effects [175]. In this system, vortices may correspond to charges, quenched disorder (pinning) to random offset charges in the islands, and vortex interactions, to the rules governing the tunnelling process. It must be said, however, that there is an upper limit for the islands charges, differently from the vortex scenario, where the pinning strength is virtually unbounded [178]. A rough approximation of our vorticial earthquake experiment would be to apply a voltage *to the ground plane* (i.e., a pinningless medium in the vorticial system), and measure the "charge avalanches" *at the islands arrangement.*

5. Critical State and Cellular Automata

Computer simulations have become more and more popular in contemporary science. Hence, it is not surprising that the critical state has been extensively studied by means of *MonteCarlo simulations* (particularly in connection to flux creep phenomena, but also with avalanche dynamics) [179] and *molecular dynamics simulations, MD* [60,63]. The latter is potentially the ultimate weapon in vortex-state simulations, since it consists in following the dynamics of any set of interacting particles –vortices in our case– by integrating their equations of motion [180]. However, MD simulations have the important handicap that they usually require strong computational tools if big systems are to be tackled. *Cellular automata* models (CA), on the other hand, are simpler computational models that can grasp the physical essence of many physical situations with less computer power demand ¶ A CA is a dynamical system where space, time and the states of the system are discrete. In the CA, each *cell* of a regular spatial lattice can have only one of a finite number of states, which is updated according to a *local rule*, i.e., depending only of the state of the cell and their neighbors in the previous time step.

We are going in this section to concentrate in a particular cellular automaton model introduced by Bassler and Paczuski in 1998 [68] which simplicity allows the exploration of several features of the critical state, specially its avalanche behavior. The model represents the vortex dynamics on a two-dimensional simple hexagonal lattice. A lattice site situated at x has a pinning energy randomly chosen to be $V_{pin}(x) = p$ with probability q, and $V_{pin}(x) = 0$ with probability $1 - q$. Vortices are only allowed to exist at the lattice sites, each of which can contain $m(x)$ vortices. The upper section of Figure 23 shows an example accounting for a few lattice sites, which are represented by open circles, while the dots represent vortices. Vortices at site x of the figure can move to site y only if the "force" defined as

¶Bak and coworkers' model for SOC mentioned in section 3 was a CA!

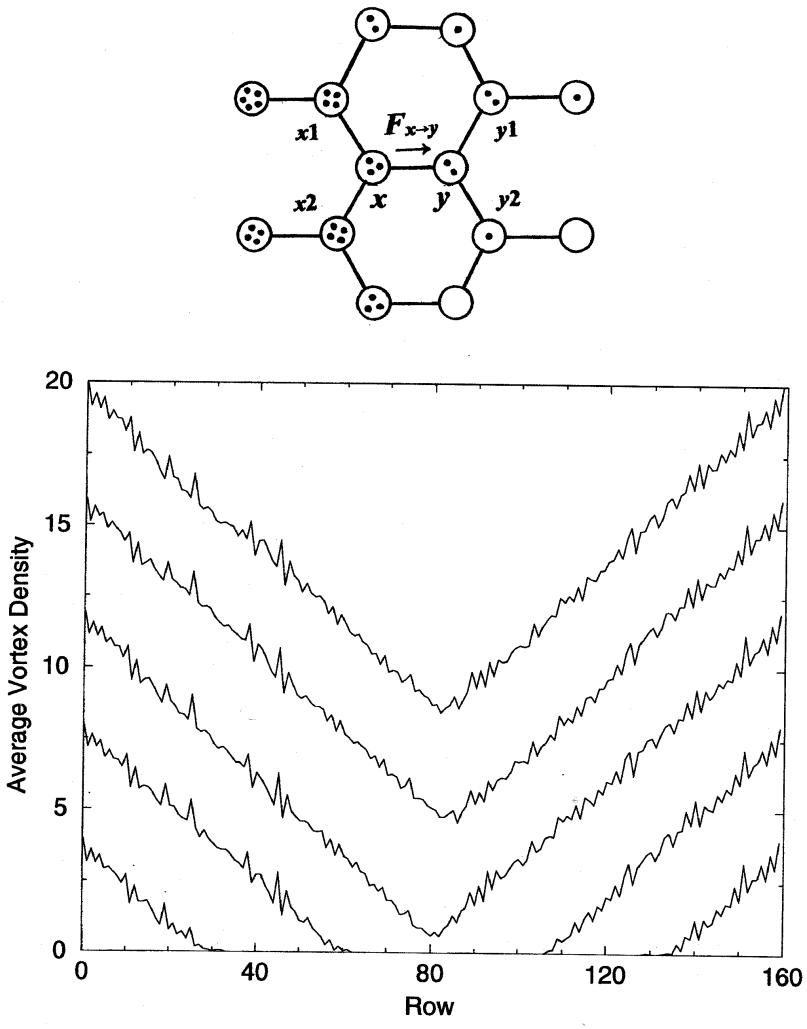

Figure 23: Illustration of the cellular automaton network proposed by Bassler and Paczuski [68] to simulate the critical state of type II superconductors. The open circles represent the network sites, and the black dots, vortices. Lower section: An example of critical state profiles for increasing magnetic field obtained through the cellular automaton.

$$F_{x\to y} = V_{pin}(y) - V_{pin}(x) + [m(x) - m(y) - 1] + r[m(x1) + m(x2) - m(y1) - m(y2)] \quad (31)$$

is greater than zero. In the above expression, r is a measure of the effect of the x and y sites nearest neighbors, namely $x1$, $x2$, $y1$ and $y2$ (In the specific example of Figure 21, assuming $V_{pin}(x) = V_{pin}(y)$ and $r = 0.2$, we obtain $F_{xy} = 1$). All sites are updated in paralell, and only one vortex from a particular site is allowed to move at each update. Then, if $F_{x\to y} > 0$, one vortex jumps from x to y. If *two* directions are unstable when calculating the force for a given x, it jumps to one of them selected at random.

The increase of the external magnetic field is represented by the random addition of vortices to the system through its left boundary. Periodic boundary conditions are applied to the top and bottom of the lattice. The vortices reaching the right boundary are removed (they "fall out" of the system), and no vortices are allowed to abandon it through the left boundary.

Note that the different forces acting on vortices are not calculated through equations (14)-(17) –as expected from a MD approach–. Instead, they are represented by simple CA rules chosen with physical intuition. For example, the first two terms at the right hand of the force given by expression 31 indicate that the vortices tend to move from weak to strong pinning centers, while the rest of the terms indicate that they tend to move in the direction of the (local) flux gradient due to intervortex repulsion. A more subtle matter is to discuss if the model is able to deal with the viscous force associated to vortex movement, introduced in section 2. In fact, the intrinsic discreteness of the CA implies eventual vortex "stops" at a few "pinnningless" sites in its way from one pinning center to the next one: in my opinion, this somehow mimics the finite velocity of vortices during *flux flow*.

The lower part of Figure 23 displays a typical sequence of vortex density profiles for increasing values of the external field obtained through the model described. A relatively small density of sites has been selected in the example to illustrate the vortex density fluctuations along the profile, which reproduces accurately the predictions of Bean's critical state model, illustrated in Figures 6 and 7.

But the most exciting use of the CA model is the possibility to examine *how* the critical state is reached. For that purpose, Bassler and Paczuski excited their CA by adding a vortex to a random site at the left boundary of the system, resembling an increasing magnetic field in the outside. The lattice sites were then continually updated until no more unstable sites persisted. This process was called a *vortex avalanche. The avalanche size was defined as the number of topplings following a vortex addition, while the avalanche duration was defined as the number of updatings necessary to complete one avalanche.* Once the lattice was again stable, a new vortex was added.

Figure 24a shows the times series of vortices falling off the right edge of an approximately squared system of $L = 200$ size, and parameters $r = 0.1$, $p = 5$ and $q = 0.1$, which qualitatively resembles the result of the 1995' experiment by Field et al [52] represented in Figure 13, although one must be aware of the fact that *flux* avalanches are not *directly* shown there. The following finite

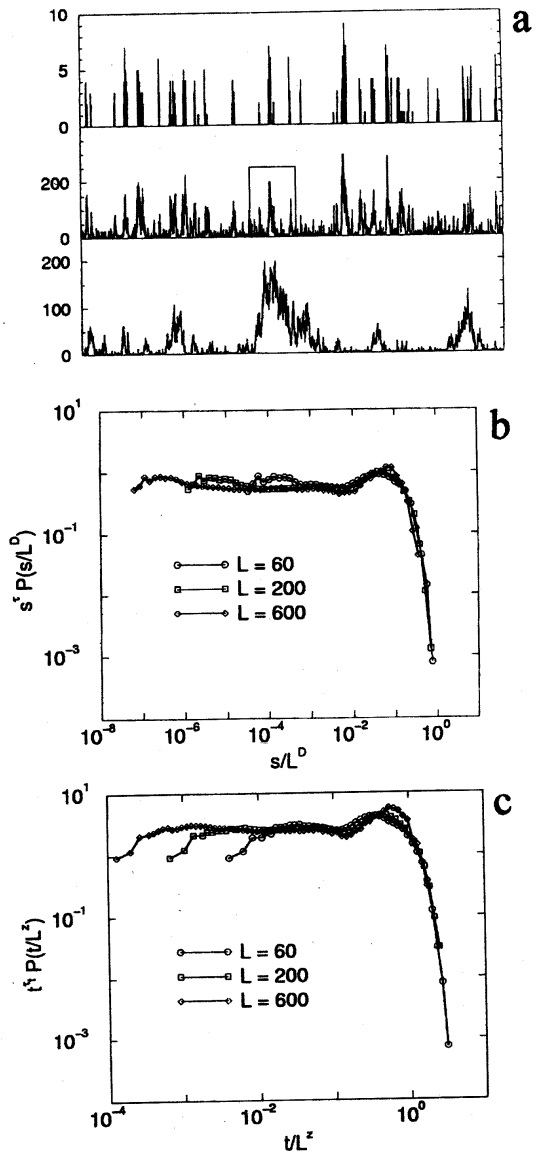

Figure 24: Top graph: temporal series of vortex avalanches reported by Bassler and Paczuski using the cellular automaton illustrated in Figure 23 [68]. Intermediate and lower graphs: data collapse after finite size scaling of the avalanche sizes and lifetimes distributions by the same authors.

size scaling ansazt was use to analyze the avalanche sizes and durations distributions, respectively for systems of sizes $L = 60$, $L = 200$ and $L = 600$.

$$P(s, L) = s^{-\tau} f(s/L^D) \tag{32}$$

$$P(t, L) = t^{-\tau_t} f(t/L^z) \tag{33}$$

The data collapse –illustrated in Figure 24b,c– resulted in critical exponents $\tau = 1.63 \pm 0.02$, $D = 2.7 \pm 0.1$, $\tau_t = 2.13 \pm 0.08$ and $z = 1.5 \pm 0.1$. (note that no finite size scaling was necessary in [52] due to the huge size of the real vortex system). Similar results were obtained for a wide range of simulational parameters, indicating the robustness of the system, and SOC behavior. It must be pointed out that, even when many features between the experiment reported in [52] and these CA simulations are coherent, the model differs from the experiment in treating the vortices as pointlike particles, while real vortices are objects of unknown dimensionality, as previously discussed.

Bassler and Paczuski's CA has enjoyed a rapid popularity among the superconducting simulational community. Cruz and coworkers, for example [71] have applied the model to systems with a *periodic* distribution of pinning centers (which can be achieved experimentally with state-of-the-art ion bombardment techniques [181]), finding power law distributions of avalanche sizes and durations, as well as a new universality class for strong and dense periodic distributions of pinning centers.

Mohler and Stroud, on the other hand, used the CA to calculate the flux noise of a system analogous to that reported in [52], concluding that slowly applied fields produce "1/f" noise, while fast field ramps provoke a peak in the noise spectrum, in qualitative agreement with some experimental findings.

The experimentally inescapable problem of how thermal activation of vortices affect the avalanche dynamics has been tackled by Mulet and coworkers [73] by modifying the original CA with a MonteCarlo-type algorithm, which differs from the previous analytical [48,62,65] and MD [66] approaches to the subject. The central idea of Mulet and coworkers' model is that, for vortices in sites where $F_{x \to y} < 0$, there is still the possibility of motion with a "thermal" probability given by $P_{x \to y} \propto e^{-U(j)/kT}$, where $U(j)$ can follow different pinning models, and j is the local critical current density, which is proportional to the local gradient of the vortex density, as described in section 2.2.2. In the simulation, vortices are added as in [68] until the critical state is established, and then the system is allowed to relax via thermal activation. The simulations indicate power-distributed avalanches with critical exponents related to those found by Bassler and Paczuski in their original paper [68]. The results of these simulations are partially coherent with the relaxation experiments reported in reference 56. Both works agree in that power laws are lost as the temperature increase but, while in [73] many-sized avalanches are predicted from the first moments of the relaxation process, they are observed in reference 56 only at large relaxation times. The theoretical prediction in [73] comes form the fact that, in the model, a "perfect" critical state is assumed at $t = 0$. However, it must be stressed that Aegerter's experiments are performed with

a SQUID [56], so only "off-the-edge" avalanches can be detected. On the other hand, its resolution is relatively small –as the author himself states.

A more straightforward application of Bassler-Paczuski's CA is the study of the effect of a transport current in the avalanche dynamics of the critical state. A basic approach to the subject is to assume that the effect of a transport current applied perpendicularly to the magnetic field on a thin slab (i.e., entering into the page in diagram 3 of Figure 7) is to "tilt" the field boundary conditions relative to the ones corresponding to the fully penetrated critical state at zero transport current [98]. Then , the effect of the transport current increase would be to add or release vortices asymetrically at the boundaries, and let the CA rules to "take charge" of the dynamics [182].

Curiously enough, most of the molecular dynamics simulations of vortices in the presence of a transport current assume a uniform Lorentzlike force acting on each vortex. The sandpile model for this would be the "rotating drum" experiment, in which a box of sand is slowly tilted [119]. This is not the approach followed in the CA model described in the last paragraph. In fact, its sandpile analogue would be to lower, for example, the right vertical wall of the box containing the "V" sandpile depicted in Figure 10a, as new sand is added at the left wall (which height would be increased to support the increasing left shoulder of the pile).

Finally, I will suggest some further qualitative ideas that may be implemented with the Bassler-Paczuski's CA, and may help the understanding of some properties of the critical state of type II superconductors.

A simple modification of the algorithm would be to establish a rule for the diminishing of the pinning potential as the vortex number at a given site increases, in order to resemble the field dependence of the critical current density in real superconductors. This should produce curved flux profiles, as those obtained, for example, from Kim's critical state model [45]. It would also eventually destroy SOC dynamics.

A less trivial modification of the algorithm would allow simulation of flux jumps. As we have seen above, they constitute an important experimental issue to rule out when the objective is to measure only the "dynamically driven" flux avalanches [53,54,58]. Including in the CA algorithm both kinds of flux avalanches may be useful to have an idea of their interaction. One qualitative approach of flux jumps could be to establish a maximum local rate of vortex topplings in the original CA algorithm (i.e., a maximum dissipation due to vortex movements that the sample can stand without increasing their temperature). If this maximum is reached, the pinning strengths of that region would be lowered by a certain factor (i.e., as the temperature increases due to excess flux motion, the local critical current density decreases). This would imply a "catastrophic" enter of flux into the sample (i.e., a flux jump). The values of the different parameters of the new automaton would represent those relevant to flux jumps: specific heat, thermal conduction, temperature dependence of the critical current density, etc. Observe that this idea does not imply a MC-flavored simulation of thermal activation like in [73].

Although surely much more computing-time consuming, some ideas can be suggested for approaching the *dimensionality* of real vortices with the use of Bassler-Paczuski CA. It is perhaps

a variation of the "superconducting-earthquake" experiment proposed in the last section the one most easily reproducible with the CA. The key modification would be to use *two* paralell lattices instead of one, with the external field applied perpendicular to the lattices. Then, the force formula (32) should be modified to account for the interaction between vortices –or vortex sections– *located on different lattices. One simple possibility is to add a term expressing the "preference" of vortices to occupy sites on one network directly above (or below) occupied sites in the paralell plate.* A first step to implement such idea is to define the forces at the upper and lower networks, as:

$$\begin{aligned} F^u_{x\to y} &= V_{pin}(y)^u - V_{pin}(x)^u + [m(x)^u - m(y)^u - 1] \\ &\quad + r^u[m(x1)^u + m(x2)^u - m(y1)^u - m(y2)^u] - cm(x)^l \end{aligned} \tag{34}$$

$$\begin{aligned} F^l_{x\to y} &= V_{pin}(y)^l - V_{pin}(x)^l + [m(x)^l - m(y)^l - 1] \\ &\quad + r^l[m(x1)^l + m(x2)^l - m(y1)^l - m(y2)^l] - cm(x)^u \end{aligned} \tag{35}$$

where the superscripts "u" and "l" refer to the upper and lower networks, respectively, and c *is the inter-network or inter-layer coupling constant.* Firstly, we would examine the critical state dynamics at both networks by adding vortices at their boundaries. Once established the critical states –which should be quite similar at both networks– we would mimic the injection of an increasing transport current in the upper plate by "slowly tilting" *there* the boundary conditions, and examine the avalanche dynamics *at the lower plate.* The coupling constant, c, might be able to tune interesting *dynamic phases* in the style of [183]! . This simulation, however, best reproduces a flux transformer-like experiment *in which the superconducting films are substituted by infinite slabs*: it is well known that the vortex distribution of *films* in perpendicular applied fields can be extremely complex due to strong demagnetizing effects [145,184], and their modeling is eventually beyond the original Bassler-Paczuski CA model, at least close enough to the sample boundaries. However, the case of the pancake-vortex dynamics in layered supercondcutors might be easier to approach, since it basically consists in *many* paralell CA networks, which helps to get rid of extreme demagnetizing effects.

A further variation of the Bassler-Paczuski CA could be also applied to simulate charge transport in mesoscopic structures of the kind described at the end of section 4. The lattice sites would resemble very closely the metallic dots in which charges are confined, the vortices would now represent charges, and the pinning strengths would be substituted by the random offset voltages at the islands. Finally, the new force would depend on the potential difference between adjacent islands, which, in turn, would be a function of their charges. Then, if $V_i > V_j + constant$ [177], charge would be transferred from site i to site j. Otherwise, no transfer would take place. Even when these ideas are very preliminar, they could be refined to study the avalanche behaviour of such mesoscopic systems, which, as a matter of fact, has not been directly probed in the experiment.

After so many examples of how the road between sand and vortex piles can be followed in both directions –including *detours* to other systems–, we could state a final question: why not

substitute vortices for grains, and use the Bassler-Paczuski CA for simulating avalanches in some sandpile experiments?

6. Conclusion

Experiments in vortex avalanches have demonstrated the validity of the sandpile mechanical analogue to understand some dynamic properties of the critical state in type II superconductors. How far this analogy can be exploited is still an open question. The temperature-dependent change in behavior of the superconducting critical state from power-law to peaked vortex size distributions observed in some experiments –possibly related to vortex inertia– is one of the most intriguing aspects of the problem. State-of-the-art experimental techniques for the measurement of the *local* magnetic induction have allowed, in the last years, to get a preliminary picture of the spatio-temporal correlations of vortex avalanches, but more work should be done, specially regarding the correlations along the direction paralell to the applied field. A variety of vortex-avalanche experiments exploring different geometries and the inclusion of transport currents is waiting for future efforts. Some experiments on sandpiles and magnet arrangements might also help to understand the dynamics of vortex avalanches. Cellular automata (CA) models –which have already shown their effectiveness in approaching vortex avalanches– constitute an elastic tool to tackle some of these problems, if local rules are carefully selected on a solid phenomenological background. There is no doubt that the zoology of "vorticial CA's" will grow fast in the next years.

Acknowledgments

I would like to thank the Editors for the liberty I enjoyed to choose the subject of this article and their continued encouragement, particularly from L.M. Gaggero. I am indebted to my former student and colleague R. Mulet for being my partner in the difficult task of tackling new scientific problems in a Third World environment along many years, and, specifically, for compulsive arguments on avalanche dynamics. I highly appreciate discussions with R. Cruz, A.J. Batista, O. Ramos, A. Vázquez, O. Sotolongo, K. Bassler, M. Paczuski, G. Reiter, A. Rimberg and Y. Paltiel; scientific advice from C.W. Chu, J.R. Clem, H. Herrmann and E. Zeldov, and experimental details provided by E. Nowak and K. Behnia. I also thank the critical reading of the manuscript by G. Reiter, R. Mulet and K.Bassler, as well as the latter and G. Gunaratne for cooperation in Figure 10. Material support during the last stage of this work is gratefully acknowledged to the ICSC-World Laboratory, the Physics Department at the University of Houston, and the Texas Center for Superconductivity. Thanks to my wife and family, writing this paper has not seriously damaged my mental health.

References

1. J.C. Maxwell: "The theory of molecular vortices applied to statical electricity". *Philosophical Magazine*, January-February 1892
2. H. Kammerlingh-Onnes : "Sur les résistances électriques". En la *Théorie du rayonnement et les quanta, rapports et discussions de la réunion tenue Bruxelles*, du 30 octobre au 3 novembre 1911 sous les auspices de M.E. Solvay, pgs 304-312
3. For an excellent review, see D.R. Tilley and J. Tilley *Superfluidity and Superconductivity* (3rd. ed.), Adam Hilger, Bristol and New York, 1990
4. J. Bardeen, L.N. Cooper and J.R. Schrieffer, *Phys. Rev.* **108** (1957) 1175-1204
5. F. London and H. London, *Proc. Roy. Soc.* **A149** (1935) 71
6. W. Meissner and R. Ochsenfeld, *Naturwiss* **21** (1933) 787
7. R. Doll and M. Näbauer, *Phys. Rev. Lett.* **7** (1961) 51-52
8. B.S. Deaver, Jr. and W.M. Fairbank, *Phys. Rev. Lett.*, **7** (1961) 43-46
9. B.D. Josephson, *Phys. Lett.* **1** (1962) 251-253
10. P.W. Anderson and J.M. Rowell, *Phys. Rev. Lett.* **10** (1963) 230-232
11. P.W. Anderson, in *Lectures on the manybody problem*, Ravello, 1963 (E.R. Caianello, Ed.) vol. 2, Academic, 1964, p 113-135
12. D.B. Sullivan and J.E. Zimmerman, *Am. J. Phys.* **45** (1974) 429-433
13. V.L. Ginzburg and L.G. Landau, *Zh. Eksp. Teor.Phys.* **20** (1950) 1064
14. V.L. Ginzburg and L.P. Pitaevskii, *Zh. Eksp. Teor. Fiz.* **34** (1958) 1240
15. A.A. Abrikosov *Zh. Exsp. Teor. Fiz.* **32** (1957) 1442
16. U. Essman and H. Träuber. *Phys. Lett.* **24A** (1967) 526
17. T.P. Orlando and K.A. Delin *Foundations of Applied Superconductivity*, Addison-Wesley, 1991.
18. L. Onsager, *Nuovo Cimento* **6** (1949) 249, H.E. Hall and W.F. Vinen, Phil. Mag. **46** (1955) 546
19. M. Tinkham *Introduction to Superconductvity* McGraw-Hil, 1975
20. V.A. Kozlov and A.V. Samokhvalov, *JETP Lett.* **53** (1991) 158
21. V.A. Kozlov and A.V. Samokhvalov, *Physica C* **213** (1993) 103
22. Y. A. Genenko, *Phys. Rev. B* **49** (1994) 6950
23. R. Mulet and E. Altshuler, *Physica C* **252** (1995) 295-302
24. F. Pérez-Rodríguez, A. Peérez- González, J.R. Clem, G. Gandolfini and M.A.R. LeBlanc, *Phys. rev. B* **56** (1997) 3473
25. E. Altshuler and R. Mulet, *Physica C* **292** (1998) 39-47
26. J. Bednorz and K.A. Müller, *Z. Phys.* **B64** (1986) 189
27. M. Wu, J. Ashburn, C. Torng, O. Hor, R. Meng, L. Gao, Z. Huang and C.W. Chu, *Phys. Rev. Lett.* **58** (1987) 908
28. H. Maeda, Y. Tanaka, M. Fukutomi, and T. Asano, *Jpn. J. Appl. Phys. Lett.* **27** (1988) 209
29. Z. Sheng and A. Hermann, *Nature* **332** (1988) 55
30. A. Schilling, M. Cantoni, J.D. Guo, H.R. Ott, *Nature* **363** (1993) 56
31. L.N. Bulaevskii, Zh. Eksp. Teor. Fiz. **64** (1973) 2241
32. K.B. Efetov, Zh. Eksp. Teor. Fiz. **76** (1979) 1781
33. J.R. Clem and M.W. Coffey, Phys. Rev. **B42** (1990) 6209
34. J.P. Carton, J. Phys. I (Paris) **1** (1991) 113
35. S.N. Artemenko and A.N. Kruglov, *Phys. Lett.* **A 143** (1990) 485
36. M.V. Feigel'man, V.B.Geshkenbein and A.I. Larkin, *Physica C* **167** (1990) 17
37. A. Buzdin and D. Feinberg, *J. Phys.* (France) **51** (1990) 1971
38. J.R. Clem, *Phys. Rev.* **B43** (1991) 7837
39. K.H. Fischer, *Physica C* **178** (1991) 161

40. S. Chakravarty, B.I. Ivlev and Yu.N. Ovchinnikov, *Phys. Rev. B* **42** (1990) 2143
41. L.N. Bulaevskii, M. Ledvij and V.G. Kogan, *Phys. Rev. B* **46** (1992) 366
42. J.Bardeen and M.J.Stephen, *Phys. Rev. A* **14**0 (1965) 1197
43. A.M. Campbell and J.E. Evetts, *Adv. Phys.* **72** (1972) 199
44. Ch. Bean, *Rev. Mod. Phys.* **30**, 31 (1964)
45. Y.B. Kim, C.F. Hempstead and A.R. Strnad, *Phys. Rev. Lett.* **9** (1962) 306; P.W. Anderson and Y.B. Kim, *Rev. Mod. Phys.* **36** (1964) 39; Y.B. Kim, C.F. Hempstead and A.R. Strnad, *Rev. Mod. Phys.* **36** (1964) 43
46. W.A. Fietz, M.R. Beasley, J. Silcox and W.W. Webb, *Phys. Rev. A* **136** (1964) 335
47. See, for example: A.M. Campbell and J.E. Evetts, *Adv. Phys.* **72** (1972) 199; H. Ullmaier *Irreversible properties of type II superconductors*, Springer, Berlin, 1975; K. Tachikawa, K. Kitazawa, H. Maeda and T. Mstsushita (eds.) *Critical state in superconductors*, World Scientific, 1995.
48. X.S. Ling, D. Shi and J.I. Budnik, *Physica C* **185-189** (1991) 2181
49. Z. Koziol, P.F. de Chatel, J.M. Franse, Z. Tarnawski and A.A. Menovsky, *Physica C* **212** (1993) 133
50. G.T. Seidler, C.S. Carrillo, T.F. Rosenbaum, U. Welp, G.W. Crabtree and V.M. Vinokur, *Phys. Rev. Lett.* **70** (1993) 2814
51. P. Liderer, J. Boneberg, P. Brüll, V. Bujok and S. Herminghaus, *Phys. Rev. Lett.* **71** 2646; C.A. Durán, P.L. Gammel, R.E. Miller and D.J. Bishop, in *Critical state in superconductors*, K. Tachikawa, K. Kitazawa, H. Maeda, T. Matsushita (eds.), World Scientific, 1995 (p. 16); B-U. Runge, U. Bolz, J. Eisenmenger and P. Leiderer, paper presented at M2S-HTSC-VI, Houston, Texas, feb. 20-25, 2000.
52. S. Field, J. Witt and F. Nori, *Phys. Rev. Lett.* **74**(1995) 1206
53. R.J. Zieve, T.F. Rosenbaum, H.M. Jaeger, G.T. Seidler, G.W. Crabtree and U. Welp, *Phys. Rev. B* **53** (1996) 11849
54. E.R. Nowak, O.W. Taylor, L. Liu, H.M. Jaeger and T.J. Selinder, *Phys. Rev. B* **55** (1997) 11702
55. K. Kawashima, *Phys. Rev. B* **58** (1998) 490
56. C.M. Aegerter, *Phys. Rev. E* **58** (1998) 1438
57. P. Esquinazi, A. Setzer, D. Fuchs, Y. Kopelevich, E. Zeldov and C. Assmann, *Phys. Rev. B* **60** (1999) 12454
58. K. Behnia, C. Capan, D. Mailly and B. Etienne. cond-mat/9902334 (25 feb 1999)
59. P.G. DeGennes *Superconductivity of metals and alloys.* Benjamin, New York, 1996.
60. O. Pla and F. Nori, *Phys. Rev. Lett.* **67** (1991) 919
61. X.S. Ling and J.I. Budnik, in *Magnetic susceptibility of superconductors and other spin systems* ed. R.A. Hein, T.L. Francavilla and D.H. Liebenberg, Plenum, New York, 1991 (p. 377)
62. C. Tang, *Physica A* **194** (1993) 315
63. R.A. Richardson, O. Pla and F. Nori, *Phys. Rev. Lett.* **72** (1994) 1286
64. C. Reichhardt, C.J. Olson, J. Groth, S. Field and F. Nori, *Phys. Rev. B* **52** (1995) 10441
65. E. Bonabeau and P. Lederer. *Phys. Rev. B* **52**(1995) 494
66. S. Spencer, H.J. Jensen, *Physica C* **264** (1996) 95
67. R. Mulet and E. Altshuler, *Physica C* **281** (1997) 317
68. K.E. Bassler and M. Paczuski, *Phys. Rev. Lett.* **81** (1998) 3761
69. R. Prozorov and D. Giller, cond-mat/9901344v2
70. G. Mohler and D. Stroud, *Phys. Rev. B* **60** (1999) 9738
71. R. Cruz, R. Mulet and E. Altshuler, *Physica A* **275** (1999) 15
72. K.E. Bassler, M. Paczuski and G. Reiter, *Phys. Rev. Lett.* (15 November, 1999)
73. R. Mulet, R. Cruz and E. Altshuler, preprint (2000)
74. Y.B. Kim, C.F. Hempstead and A.R. Strnad, *Phys. Rev. Lett.* **9** (1962) 306

75. P.W. Anderson, *Phys. Rev. Lett.* **9** (1962) 309
76. P.W. Anderson and Y.B. Kim, *Rev. Mod. Phys.* **36** (1964) 39
77. E. Altshuler et al, unpublished (1990)
78. M.R. Beasley, R. Labush and W.W. Webb, *Phys. Rev.* **181** (1969) 682
79. M.V. Feigel'man, V.B. Geshkenbein, A.I. Larkin and V.M. Vinokur, *Phys. Rev. Lett.* **63** (1989) 2303
80. E. Zeldov, N.M. Amer, G. Koren, A. Gupta, R.J. Gambino and M.W. McElfresh, *Phys. Rev. Lett.* **62** (1989) 3093
81. Y. Yeshurum and A.P. Malozemoff, *Phys. Rev. Lett.* **60** (1988) 2202
82. Y. Yeshurum, A.P. Malozemoff and A. Shaulov, *Rev. Mod. Phys.* **68** (1996) 911
83. E. Altshuler, R. Cobas, A.J. Batista-Leyva, C. Noda, L.E. Flores, C. Martínez and M.T.D. Orlando, *Phys. Rev. B* **60** (1999) 3673
84. B.B. Goodman and M. Wertheimer, *Phys. Lett.* **18** (1965) 236
85. S.H. Goedmoed, C. van Kolmeschate, J.W. Metselaar and D. DeKlerk, *Physica* **31** (1965) 537
86. S.H. Goedmoed, C. van Kolmeschate, P.H. Kes and D. DeKlerk, *Physica* **32** (1966) 1183
87. P.S. Swartz and C.P. Bean, *J. Appl. Phys.* **39** (1968) 4991
88. J.C. Levet, M. Potel, P. Gougeon and H. Noel, *Nature* **331**(1988)307
89. J.L. Tholence, H. Noel, J.C. Levet, M. Potel and P. Gougeon, *Solid State Commun.* **65** (1988) 1131
90. M. Guillot, M. Potel, P. Gougeon, H. Noel, J.C. Levet, G. Chouteau and J.L. Tholence, *Phys. Lett.* **A 127** (1988) 363
91. M. Guillot, J.L. Tholence, O. Laborde, M. Patel, P. Gougeon, H. Noel and J.C. Levet, *Physica C* **162-164** (1989) 361
92. K. Chen, S.W. Hsu, T.L. Chen, S.D. Lan, W.H. Lee and P.T. Wu, *Appl. Phys. Lett.* **56** (1990) 2675
93. K. Chen, Y.C. Chen, S.W. Hsu, W.H. Lee, and P.T. Wu, *Physica C* **173** (1991) 227
94. A. Gerber, J.N. Li, Z.Z. Tarnawsky, J.J.M. Franse and A.A. Menovsky, *Phys. Rev. B* **49** (1993) 6047
95. L. Gao, Y.Y. Xue, R.L. Meng and C.W. Chu preprint No. 93:076 (1993), Texas Center for Superconductivity.
96. K.H. Müller and C. Andrikidis, *Phys. Rev. B* **49** (1994) 1294
97. L. Legrand, I. Rosenman, R.G. Mints, G. Collin and E. Janod, *Europhys. Lett.* **34** (1996) 28
98. M.N. Wilson *Superconducting magnets*, Clarendon Press, Oxford, 1983
99. C. Coulomb, in *Memoir de Mathematique et de Physique*, Vol. 7, Academie de Sciences, L'Imprimerie Royale, Paris (1773), p.343
100. M. Faraday, *Phil. Trans. R. Soc. London* **52** (1831) 299
101. O. Reynolds, *Philos. Mag.* **20** (1885) 469
102. D. Bideau and J.A. Dodds (eds.) *Physics of Granular Media*, Les Housches Series, Nova Science Publishers, 1991
103. H.M. Jaeger and S.R. Nagel, *Science* **255** (1992) 1523
104. R.P. Behringer, *Nonlinear Science Today* **3** (1993) 1
105. D. Bideau and A. Hansen (eds.) *Disorder and Granular Media*, Random Materials and Processes Series, North Holland, New York, 1993
106. H.M. Jaeger, J.B. Knight, C.H. Liu and S.R. Nagel, *Mater. Res. Bull.* **19** (1994) 25
107. A. Mehta (ed.) *Granular Matter an Interdisciplinary Approach*, Springer-Verlag, New York, 1994
108. A. Mehta and G.C. Barker, *Rep. Prog. Phys.* **57** (1994) 383
109. R.P. Behringer, *Proc. MRS* **367** (1995) 461
110. H.H. Hayakawa, H. Nishimori, S. Sasa and Y.H Taguchi, *Jpn. J. Appl. Phys.* **34** (1995)

397
111. H.M. Jaeger, S.R. Nagel and R.P. Behringer, *Rev. Mod. Phys.* **68** (1996) 1259
112. J. Duran *Physics of Granular Materials*, Springer Verlag, New York, 1999
113. L.P. Kadanoff, *Rev. Mod. Phys.* **71** (1999) 435
114. P.G. deGennes, *Rev. Mod. Phys.* **71** (1999) S374
115. H.J. Herrmann, *Physica A*, **263** (1999) 51
116. P. Bak, C. Tang and K. Wiesenfeld, *Phys. Rev. Lett.* **59**, 381 (1987); C. Tang and P. Bak, *Phys. Rev. Lett.* **60**, 2347 (1988); M. Paczuski and S. Boettcher, *Phys. Rev. Lett.* **77**, 111 (1996)
117. J.J. Alonso and H.J. Herrmann, *Phys. Rev. Lett.* **76** (1996) 4911
118. E. Altshuler, O. Ramos, C. Martínez, L.E. Flores and C. Noda, Preprint (1999)
119. H.M. Jaeger, C.H. Liu and S.R. Nagel, *Phys. Rev. Lett.* **62** (1989) 40
120. C.S. Campbell and C.E. Brennen, J. Fluid. Mech. **151** (1985) 167; S.F. Edwards and R.B.S. Oakeshott, *Physica A* **157** (1989) 1080; A. Mehta and S.F. Edwards, *Physica A* **157** (1989) 1091; H.M. Jaeger and S.R. Nagel, Science **255** (1992) 1523; H.J. Herrmann, in *Disorder and Granular Media* (Bideau and Hansen, eds.), North-Holland, Amsterdam, 1993 (pag. 305).
121. J.C. Williams, Powder Techn. **15** (1976) 245; A. Rosato, K.J. Strandburg, F. Prinz and R.H. Swendsen, *Phys. Rev. Lett.* **58** (1987) 1038; *Powder Techn.* **48** (1986) 239; P.K. Haff and B.T. Werner, *Powder Techn.* **49** (1986) 59; P. Devillard, *J. Physique* **51** (1990) 369; R. Jullien, P. Meakin and A. Pavlovitch, *Phys. Rev. Lett.* **69** (1992) 640;
122. P. Bak "How *Nature* works", Springer Verlag, New York, 1996
123. L.P. Kadanoff, S.R. Nagel, L. Wu and S. Zhou, *Phys. Rev. A*, **39**, 6524 (1989)
124. See, for example, Wilde and Singh *Statistical Mechanics*, Wiley, New York, 1998.
125. G.A. Held, D.H. Solina, D.T.Keane, W.J. Haag, P.M. Horn and G. Grinstein, *Phys. Rev. Lett.* **65**, 1120 (1990)
126. M. Bretz, J.B. Cunningham, P.L. Kurezynski and F. Nori, *Phys. Rev. Lett.* **69** (1992) 2431
127. P. Evesque, *Phys. Rev. A* **43** (1991) 2720
128. J.Rosendahl, M. Vekic and J. Kelley, *Phys. Rev. Lett.* **47**, (1993) 1401
129. P. Evesque, D. Fargaix, P. Habib, M.P. Luong and P. Porion, *Phys. Rev. E* (1993) 2326
130. S.K. Grumbacher, K.M. McEwen, D.A. Halverson, D.T. Jacobs and J. Linder, *Am. J. Phys.* **61**, (1993) 329
131. J. Rodendahl, M. Vekic and J.E. Rutledge *Phys. Rev. Lett.) (***73** (1994) 537
132. V. Frette, K.Christensen, A. Malthe-Søslashrensen, J. Feder, T. Jossang and P. Meakin, *Nature*, **379**, 49 (1996)
133. K. Christensen, A. Corral, V. Frette, J. Feder and T. Jøssang, *Phys. Rev. Lett.* **77** (1996) 107
134. Y.B. Kim, C.F. Hempstead and A.T. Strnad. *Phys. Rev.* **131**(1963)2468
135. C. Heiden and G.I. Rochlin, *Phys. Rev. Lett.* **21** (1968) 691
136. C.R. Wischmeyer, *Phys. Lett.* **19** (1965) 543-545
137. A.I. Larkin and Yu.N. Ovchinnikov, *Zh. Eksp.Teor.Fiz.* **65** (1973) 1704
138. A.I. Larkin and Yu.N. Ovchinnikov, *J. Low Temp. Phys.* **34**(1979)409-427
139. G. Blatter, V.B. Geshkenbein and V.M. Vinokur, *Phys. Rev. Lett.* **66** (1991) 3297
140. G. Blatter, M.V. Feigel'man, V.B. Geshkenbein, A.I. Larkin and V.M. Vinokur, *Rev. Mod. Phys.* **66** (1993)1125
141. R.J. Donnelly, *Cryogenics* in Physics Vade Mecum, edited by H.L. Anderson. AIP, 1981.
142. M. Konczykowsky, L.Burchalov, Y. Yeshurun and F. Holtzberg, *Supercond. Sci. Tech.* **4** (1991) S33
143. N. Chikumoto, M. Konczykowsky, N. Motohira, and A.P. Malozemoff, *Phys. Rev. Lett.*

69 (1992) 1260
144. M. Darwin, J. Deak, L. Hou, M. McElfresh, E. Zeldov, J.R. Clem and M. Idenbom, *Phys. Rev. B* **48** (1993) 13192
145. E. Zeldov, A.I. Larkin, V.B. Geshkenbein, M. Konczykowsky, D. Majer, B. Khaykovich, V.M. Vinokur and H. Shtrikman, *Phys. Rev. Lett.* **73** (1994) 1428
146. Y. Abufalia, A. Shaulov, Y. Wolfus, R. Prozorov, L. Burlachkov, Y. Yeshurun, D. Majer, E. Zeldov and V.M. Vinokur, *Phys. Rev. Lett.* **75** (1995) 2404
147. Y. Abufalia, D. Giller, Y. Wolfus, A. Shaulov, Y. Yeshurum, D. Majer, E. Zeldov, J.L. Peng and R.L. Greene, *J. Appl. Phys.* **81** (1997) 4944
148. Y. Abufalia, M. McElfresh, A. Shaulov, Y. Yeshurum, Y. Paltiel, D. Majer, H. Strikman and E. Zeldov, *Appl. Phys. Lett.* **72** (1998) 2891
149. Y. Abufalia, Y. Wolfus, M. McElfresh, A. Shaulov, Y. Yeshurum, Y. Paltiel, H. Shtrikman and E. Zeldov, *J. Appl. Phys.* **85** (1999) 5471
150. R. Busch, G. Ries, H. Werthner, G. Kreiselmeier and G. Saemann-Ischenko, *Phys. Rev. Lett.* **69** (1992) 522
151. H. Safar, P.L. Gammel, D.J. Bishop, D.J. Mitzi and A. Kapitulnik, *Phys. Rev. Lett.* **68** (1992) 2672
152. H. Safar, P.L. Gammel, D.A. Huse, S.N. Majumdar, L.F. Schneemeyer, D.J. Bishop, D. López, G. Nieva and F. de la Cruz, *Phys. Rev. Lett.* **72** (1994) 1272
153. Y.M. Wan, S.E. Hebboul and J.C. Garland, *Phys. Rev. Lett.* **72** (1994) 3867
154. D. López, G. Nieva, F. de la Cruz, H.J. Jensen and D. O'Kane, *Phys. Rev. B* **50** (1994) 9684
155. F. de la Cruz, D. López and G. Nieva, *Phil. Mag. B* **70** (1994) 773
156. Yu. Eltsev, W. Holm and Ö. , *Phys. Rev. B* **49** (1994) 12333; *Physica C* **235-240** (1994) 2605
157. Yu. Eltsev and Ö. Rapp, *Phys. Rev. B* **51** (1995) 9419
158. T.S. Lee, N. Missert, L.T. Sagdahl, J.R. Clem, K. Char, J.N. Eckstein, D.K. Fork, L. Lombardo, A. Kapitulnik, L.F. Scheemeyer, J.V. Waszczak and R.B. Van Dover, *Phys. Rev. Lett.* **74** (1995) 2796
159. S.S. Manna and D.V. Khakdhar, *Phys. Rev. E* **58** (1998) 39-74
160. E. Nowak, private communication
161. P.H. Kes, in J. Evetts (ed.) *Concise Encyclopedia of Magnetic and Superconducting Materials*, Pergamon Press, 1992.
162. K. Behnia, private communication.
163. B. Gutenberg and C. Richter *Seismicity of the Earth.* Princeton Univerity Press, Princeton, 1949
164. R. Burridge and L. Knopoff *Bull. Seis. Soc. Am.* **57** (1967) 341
165. P. Bak and C. Tang, *J. Geophys. Res. B* **94** (1989) 15635
166. A. Sornette and D. Sornette, *Europhys. Lett.* **9** (1989) 197
167. K. Ito and M. Matsuzaki, *J. Geophys. Res. B* **95** (1990) 6853
168. Z. Olami, H.J. Feder and K. Christensen, *Phys. Rev. Lett.* **68** (1992) 1244
169. H. Leschhorn, *Physica A* **195** (1993) 324
170. H.J. Feder and J. Feder, *Phys. Rev. Lett.* **66** (1991) 2669
171. J.M Carlson and J.S. Langer, *Phys. Rev. Lett.* **62**(1989) 2632
172. I. Giaever, *Phys. Rev. Lett.* **15** (1965) 825
173. R. Labush, *Phys. Stat. Solidi. (b)* **32** (1969) 439
174. E.H. Brandt, *Phys. Stat. Solidi (b)* **35** (1969) 1027; **36** (1969) 371
175. C. Kurdak, A.I. Rimberg, T.R. Ho and J. Clarke, *Phys. Rev. B* bf 57 (1998) 6842
176. A.J. Rimberg, T.R. Ho and J. Clarke, *Phys. Rev. Lett.* **74** (1995) 4714
177. A.A. Middleton and N.S. Wingreen, *Phys. Rev. Lett.* **71** (1993) 3198
178. A.J. Rimberg, personal communication (1999)

179. See, for example, G. Carneiro, *Phys. Rev. B* **50** (1994) 6982; R. Mulet and E. Altshuler, Phys. Stat. Solidi (b) **182** (1994) K31; R. Mulet and E. Altshuler, *Physica C* **281** (1997) 317
180. J.M. Haile *Molecular dynamics simulations*, Wiley, New York, 1992.
181. K. Harada, O. Kamimura, H. Kasai, T. Matsuda, A. Tonomura. V.V. Moshchalkov, *Science* **74** (1996) 1167
182. K. Bassler et al, unpublished (1999)
183. C. Reichhardt, C.J. Olson and F. Nori, cond-mat/9703021 (1997)
184. M. Benkraouda and J.R. Clem, *Phys. Rev. B* **53** (1996) 5716